Dosimetric effects of breathing motion in radiotherapy

Edvardsson, Anneli

2018

Dosimetric effects of breathing motion in radiotherapy

ANNELI EDVARDSSON | DEPARTMENT OF MEDICAL RADIATION PHYSICS
FACULTY OF SCIENCE | LUND UNIVERSITY

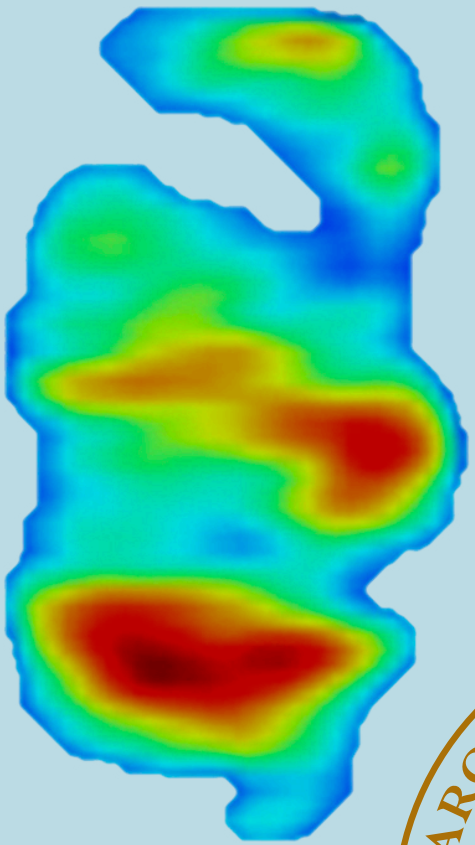

Dosimetric effects of breathing motion in radiotherapy

Anneli Edvardsson

LUND
UNIVERSITY

DOCTORAL DISSERTATION
by due permission of the Faculty of Science, Lund University, Sweden.
To be defended in the lecture hall, 3rd floor in the radiotherapy building at Skåne University Hospital, Klinikgatan 5, Lund, Friday, October 5th 2018 at 9.00 am.

Faculty opponent
Professor Tufve Nyholm
Department of Radiation Sciences, Umeå University, Umeå, Sweden

Organization LUND UNIVERSITY	Document name Doctoral Dissertation
Department of Medical Radiation Physics Clinical Sciences, Lund Faculty of Science	Date of issue 2018-10-05
Author(s) Anneli Edvardsson	Sponsoring organization

Title and subtitle Dosimetric effects of breathing motion in radiotherapy

Abstract

The goal of radiotherapy is to deliver a homogeneous high dose of radiation to a tumour while minimising the dose to the surrounding healthy tissue. To achieve this, increasingly advanced treatment techniques, such as volumetric modulated arc therapy (VMAT) and proton therapy, have been developed. However, these treatment techniques are sensitive to patient motion, such as breathing, which may degrade the dose distribution to the tumour and healthy tissue. The simultaneous movement of the tumour and treatment delivery may cause unwanted heterogeneities in the dose distribution, so-called interplay effects. Treatment during deep inspiration (DI) could mitigate the motion and lead to favourable anatomical changes in the tumour position with respect to healthy tissue. The aim of the work presented in this thesis was to investigate various effects of breathing motion on the tumour and healthy tissue dose distribution in radiotherapy.

Potential healthy tissue dose sparing using DI photon or proton therapy was investigated for left-sided breast cancer and mediastinal Hodgkin's lymphoma (HL) by performing comparative treatment planning studies. The use of DI reduced the dose to healthy tissue for left-sided breast cancer patients. It also reduced the healthy tissue dose for most mediastinal HL patients, but the benefits were more patient specific due to large variations in the disease distribution. Protons reduced the dose to healthy tissue for both left-sided breast cancer and mediastinal HL patients compared to photons, regardless of the use of DI.

A tool to simulate breathing-motion-induced interplay effects for VMAT was developed and used to investigate how interplay effects vary for different treatment scenarios. The tool was further adapted for use in a more clinical setting to investigate interplay effects for stereotactic VMAT treatment of liver metastases. Interplay effects were shown to negatively affect the dose distribution, resulting in underdosing part of the tumour. The extent of interplay effects depended on the tumour motion and treatment plan characteristics.

In conclusion, major dosimetric effects of breathing motion on radiotherapy treatment were demonstrated by the work presented in this thesis. A beneficial effect of reduced healthy tissue dose was observed when the patient used controlled DI. Furthermore, by knowing the breathing-induced motion of the tumour, the treatment delivery parameters can be selected wisely to minimise unwanted interplay effects. Knowledge of the dosimetric effects of breathing motion is important to be able to individually optimise the radiotherapy treatment.

Key words Radiotherapy, breathing motion, DIBH, interplay effects, VMAT, proton therapy, breast cancer, Hodgkin's lymphoma, liver, dosimetry, treatment planning

Classification system and/or index terms (if any)

Supplementary bibliographical information		Language English
ISSN and key title		ISBN 978-91-7753-804-2 (print) 978-91-7753-805-9 (pdf)
Recipient's notes	Number of pages	Price
	Security classification	

Dosimetric effects of breathing motion in radiotherapy

Anneli Edvardsson

LUND
UNIVERSITY

Cover: Dose distribution containing hot and cold spots from breathing-induced interplay effects for an intentionally homogeneous dose from a volumetric modulated arc therapy treatment of a liver tumour.

Faculty of Science, Lund University
Department of Medical Radiation Physics

ISBN 978-91-7753-804-2 (print)
ISBN 978-91-7753-805-9 (pdf)

Printed in Sweden by Media-Tryck, Lund University
Lund 2018

Table of Contents

Abstract

The goal of radiotherapy is to deliver a homogeneous high dose of radiation to a tumour while minimising the dose to the surrounding healthy tissue. To achieve this, increasingly advanced treatment techniques, such as volumetric modulated arc therapy (VMAT) and proton therapy, have been developed. However, these treatment techniques are sensitive to patient motion, such as breathing, which may degrade the dose distribution to the tumour and healthy tissue. The simultaneous movement of the tumour and treatment delivery may cause unwanted heterogeneities in the dose distribution, so-called interplay effects. Treatment during deep inspiration (DI) could mitigate the motion and lead to favourable anatomical changes in the tumour position with respect to healthy tissue. The aim of the work presented in this thesis was to investigate various effects of breathing motion on the tumour and healthy tissue dose distribution in radiotherapy.

Potential healthy tissue dose sparing using DI photon or proton therapy was investigated for left-sided breast cancer and mediastinal Hodgkin's lymphoma (HL) by performing comparative treatment planning studies. The use of DI reduced the dose to healthy tissue for left-sided breast cancer patients. It also reduced the healthy tissue dose for most mediastinal HL patients, but the benefits were more patient specific due to large variations in the disease distribution. Protons reduced the dose to healthy tissue for both left-sided breast cancer and mediastinal HL patients compared to photons, regardless of the use of DI.

A tool to simulate breathing-motion-induced interplay effects for VMAT was developed and used to investigate how interplay effects vary for different treatment scenarios. The tool was further adapted for use in a more clinical setting to investigate interplay effects for stereotactic VMAT treatment of liver metastases. Interplay effects were shown to negatively affect the dose distribution, resulting in underdosing part of the tumour. The extent of interplay effects depended on the tumour motion and treatment plan characteristics.

In conclusion, major dosimetric effects of breathing motion on radiotherapy treatment were demonstrated by the work presented in this thesis. A beneficial effect of reduced healthy tissue dose was observed when the patient used controlled DI. Furthermore, by knowing the breathing-induced motion of the tumour, the treatment delivery parameters can be selected wisely to minimise unwanted interplay effects. Knowledge of the dosimetric effects of breathing motion is important to be able to individually optimise the radiotherapy treatment.

Populärvetenskaplig sammanfattning

Cirka hälften av alla som drabbas av cancer i Sverige genomgår strålbehandling, där högenergetisk strålning används för att tillintetgöra cancertumören. Inför strålbehandlingen görs en datortomografiundersökning, vilket är en form av röntgenundersökning som ger snittbilder av patienten i tre dimensioner. I dessa bilder markerar en läkare det område som ska bestrålas mycket (tumören) samt de områden som ska bestrålas så lite som möjligt (frisk intilliggande vävnad). Själva behandlingen simuleras sedan i ett datorprogram, där flera olika parametrar kan justeras, så som strålslag, strålfältets storlek, form och riktning, samt strålningens energi (genomträngningsförmåga), för att ge en hög och jämn fördelning av strålningen till tumören och samtidigt minimera strålningen till den friska vävnaden. Själva behandlingen ges med en strålningsapparat som kallas linjäraccelerator, som producerar fotonstrålning, eller med en cyklotron alternativt synkrotron som producerar protonstrålning. Skillnaden mellan foton- och protonstrålning är bl.a. att protoner är laddade partiklar, som avger sin energi djupare i kroppen, och på så sätt kan styras mer precist till tumören. På senare år har mer avancerade behandlingstekniker utvecklats, där strålningen bättre koncentreras till tumörområdet så att den friska vävnaden skonas. Detta innebär att en högre mängd strålning kan ges till tumören samtidigt som risken för biverkningar av behandlingen minskar. Ett exempel på en sådan behandlingsteknik är att linjäracceleratorn roterar runt patienten samtligt som fotonstrålning levereras kontinuerligt med varierad intensitet. På så sätt ges ett litet strålningsbidrag från varje vinkel runt patienten, och dessa överlappas i tumören där mängden strålning då blir mycket stor.

Tumörer i området kring bröstkorgen rör sig när patienten andas. Under behandlingen är det viktigt att strålningen hamnar på exakt rätt ställe, vilket försvåras om tumören rör sig. Med de nya teknikerna är strålningen så väl anpassad till tumören att man riskerar att missa den om man inte tar hänsyn till tumörens rörelse. Vanligtvis utökas behandlingsmarginalen kring tumören för att säkerställa bestrålningen trots rörelse, men på bekostnad av att en större mängd frisk vävnad bestrålas. Det kan dessutom förekomma inbördes rörelser mellan bestrålningsmaskinens delar och tumören, vilket kan resultera i en ojämn fördelning av strålningen till tumören. Dessa oönskade effekter, sk interplayeffekter, förekommer trots utökad behandlingsmarginal och är svåra att förutspå då de beror på många olika behandlingsrelaterade parametrar. I nuläget finns inget kommersiellt program som beräknar interplayeffekter för en patientbehandling. I denna avhandling utvecklades därför ett verktyg för avancerade datorsimuleringar av interplayeffekter. Detta verktyg användes för att undersöka hur interplayeffekter varierar med olika behandlingsrelaterade parametrar, samt applicerades på stereotaktisk behandling av levertumörer, där en stor mängd strålning levereras vid några få behandlingstillfällen. Simuleringarna påvisade förekomsten av

interplayeffekter, vilket gav upphov till en ojämn fördelning av strålningen till tumören. Delar av tumören fick således för lite strålning, vilket skulle kunna påverka behandlingsresultatet negativt. Interplayeffekterna varierade med de olika parametrarna som simulerades och genom att välja dessa parametrar klokt, kan man således minska dessa oönskade effekter. Detta verktyg kan i framtiden användas kliniskt för att förutspå effekter av andningsrörelser för verkliga patientbehandlingar.

Det finns sätt att hantera tumörrörelser som inte kräver en ökad behandlingsmarginal och minimerar oönskade rörelseeffekter. Ett exempel är att patienten håller andan under bestrålningen. Om patienten andas in djupt kan dessutom tumören separeras från strålkänsliga organ, vilket ibland kan vara fördelaktigt. Till exempel ökar avståndet mellan bröstet och hjärtat vid djup inandning, vilket är fördelaktigt vid behandling av vänstersidig bröstcancer. I denna avhandling har behandling under djup inandning, i kombination med både foton- och protonbehandling, för vänstersidig bröstcancer och Hodgkins lymfom (cancer i lymfsystemet) undersökts. Generellt visade sig både behandling under djup inandning och protoner vara fördelaktigt med minskad strålning till hjärtat och lungorna. Dessa resultat har bidragit till klinisk implementation av en säkrare samt mer effektiv och patientvänlig teknik för behandling av bröstcancer och Hodgkins lymfom under djup inandning på Skånes universitetssjukhus, och legat till grund för utvecklingen av nationella riktlinjer. De har också bidragit till att det svenska protoncentrat Skandionkliniken, som en av de första klinikerna i världen, har behandlat en Hodgkins lymfom patient med protoner under djup inandning.

List of papers

The thesis is based on the work presented in the following papers, which are cited in the text by their associated roman numerals. The papers are appended at the end of the thesis.

I. **Comparison of doses and NTCP to risk organs with enhanced inspiration gating and free breathing for left-sided breast cancer radiotherapy using the AAA algorithm**
Edvardsson A, Nilsson MP, Amptoulach S, Ceberg S
Radiat Oncol, 2015, 10:84

II. **Respiratory gating for proton beam scanning versus photon 3D-CRT for breast cancer radiotherapy**
Flejmer AM, Edvardsson A, Dohlmar F, Josefsson D, Nilsson M, Witt Nyström P, Dasu A
Acta Oncol, 2016, 55(5):577-583

III. **Dosimetric effects of intrafractional isocenter variation during deep inspiration breath-hold for breast cancer patients using surface-guided radiotherapy**
Kügele M, Edvardsson A, Berg L, Alkner S, Andersson Ljus C, Ceberg S
J Appl Clin Med Phys, 2018, 19(1):25-38

IV. **Comparative treatment planning study for mediastinal Hodgkin's lymphoma: Impact on normal tissue dose using deep inspiration breath hold proton and photon therapy**
Edvardsson A*, Kügele M*, Alkner S, Enmark M, Nilsson J, Kristensen I, Kjellén E, Engelholm S, Ceberg S
* contributed equally to this work
Acta Oncol, 2018, DOI: 10.1080/0284186X.2018.1512153

V. **Motion induced interplay effects for VMAT radiotherapy**
Edvardsson A, Nordström F, Ceberg C, Ceberg S
Phys Med Biol, 2018, 63:085012

VI. **Breathing-motion induced interplay effects for stereotactic body radiotherapy of liver tumours using flattening-filter free volumetric modulated arc therapy**
Edvardsson A, Scherman-Rydhög J, Nilsson MP, Wennberg B, Nordström F, Ceberg C, Ceberg S
Submitted to Phys Med Biol

List of contributions

I. I contributed significantly to the planning of the study. I performed all data acquisition, treatment planning, and data analysis. I was the main author of the paper.

II. I was responsible for the parts regarding the management of breathing-induced motion. I contributed the CT data and the photon treatment plans. I reviewed and commented on the manuscript.

III. I contributed to the planning of the study. I participated in the data acquisition, the data analysis, and the writing of the paper, particularly the parts about dosimetric comparison between deep inspiration breath-hold (DIBH) and free breathing, and the dosimetric effects of intrafractional DIBH isocenter reproducibility.

IV. I contributed significantly to the planning of the study. Together with my co-first author, I performed the data acquisition, treatment planning, data analysis, and the writing of the paper.

V. I contributed significantly to the planning of the study. I participated in the development of the simulation method and performed all simulations, measurements, and data analysis. I was the main author of the paper.

VI. I contributed significantly to the planning of the study. I developed the simulation method and performed all treatment planning, simulations, and data analysis. I was the main author of the paper.

Preliminary reports

A selection of presentations at international conferences:

Reduced cardiac and pulmonary complication probabilities for breast cancer radiotherapy using respiratory gating
Edvardsson A, Nilsson MP, Amptoulach S, Ceberg S
Radiother Oncol, 2014, 111:S226-S227

Reduced doses to risk organs using enhanced inspiration gating for Hodgkin's lymphoma radiotherapy
Edvardsson A, Kügele M, Kjellén E, Engelholm S, Thornberg C, Ceberg S
Radiother Oncol, 2015, 115:S806-S807

Motion induced interplay effects for hypo-fractionated FFF VMAT treatment of liver tumours
Edvardsson A, Nordström F, Ceberg C, Ceberg S
Radiother Oncol, 2016, 119:S218

Motion-Induced Interplay Effects for Hypofractionated Volumetric Modulated Arc Therapy Treatment of Liver Tumors-Dependence on Breathing Pattern, Dose Rate, and Plan Modulation Complexity
Edvardsson A, Nordström F, Ceberg C, Ceberg S
Int J Radiat Oncol Biol Phys, 2016, 96(2):E661

Dosimetric Benefits From Deep Inspiration Proton and Photon Therapy for Hodgkin Lymphoma
Kügele M, Edvardsson A, Alkner S, Kristensen I, Kjellén E, Engelholm S, Ceberg S
Int J Radiat Oncol Biol Phys, 2016, 96(2):E662

Publications not included in this thesis

Normal tissue sparing potential of scanned proton beams with and without respiratory gating for the treatment of internal mammary nodes in breast cancer radiotherapy
Dasu A, Flejmer AM, Edvardsson A, Witt Nyström P
Phys Med, 2018, 52:81-85

The effect of systematic set-up deviations on the absorbed dose distribution for left-sided breast cancer treated with respiratory gating
Edvardsson A, Ceberg S
J Phys Conf Ser, 2013, 444:012099

Verification of motion induced thread effect during tomotherapy using gel dosimetry
Edvardsson A, Ljusberg A, Ceberg C, Medin J, Ambolt L, Nordström F, Ceberg S
J Phys Conf Ser, 2016, 573:012048

Abbreviations

3D-CRT	three-dimensional conformal radiotherapy
4DCT	four-dimensional computed tomography
AAA	anisotropic analytical algorithm
AP	anterior-posterior
CC	cranio-caudal
CI	conformity index
CT	computed tomography
CTV	clinical target volume
CTV-T	primary tumour clinical target volume
DI	deep inspiration
DIBH	deep inspiration breath-hold
DIR	deformable image registration
D_{mean}	mean dose
DVF	deformation vector field
DVH	dose-volume histogram
$D_{Y\%/cm3}$	dose to Y%/cm^3 of the volume
EIG	enhanced inspiration gating
FB	free breathing
FFF	flattening-filter free
GTV	gross tumour volume
Gy	Gray
HI	heterogeneity index
HL	Hodgkin's lymphoma
ID	integral dose
IMN	internal mammary nodes
IMPT	intensity modulated proton therapy
IMRT	intensity modulated radiotherapy

INRT	involved node radiotherapy
ISRT	involved site radiotherapy
ITV	internal target volume
LAD	left anterior descending coronary artery
linac	linear accelerator
LR	left-right
MLC	multileaf collimator
MRI	magnetic resonance imaging
MU	monitor unit
NTCP	normal tissue complication probability
OAR	organ at risk
OS	optical surface scanning
PBS	pencil beam scanning
PET	positron emission tomography
PIV	prescription isodose volume
PTV	planning target volume
RBE	relative biological effectiveness
RPM	real-time position management
SBRT	stereotactic body radiotherapy
SFUD	single field uniform dose
SOBP	spread-out Bragg peak
TCP	tumour control probability
TPS	treatment planning system
TV	target volume
VMAT	volumetric modulated arc therapy
$V_{X\%/Gy}$	volume that receives a dose ≥ X%/Gy

Introduction

During radiotherapy, patients are treated with ionizing radiation with the goal of eradicating tumour cells while sparing surrounding healthy tissue. In general, this goal is achieved by trying to deliver a homogeneous high dose to the tumour, while minimising the dose to healthy tissue as much as possible. In the past, large open fields were used to treat the patient, ensuring dose coverage of the tumour; however, it resulted in exposing large healthy tissue volumes to a high dose. Therefore, over the last few decades, different attempts have been made to reduce the healthy tissue dose, including for example, more advanced photon delivery techniques such as volumetric modulated arc therapy (VMAT), and proton therapy. These techniques enable a more conformal dose distribution to the tumour and hence reduces the dose to healthy tissue. However, they give more complex treatment plans with steeper dose gradients, making them more sensitive to patient motion, which might degrade the dose distribution to the tumour and healthy tissue. Breathing is one of the dominating patient motions and affects tumour sites in the thorax and abdomen, such as the lungs, liver, breasts, oesophagus, pancreas, and kidneys [1].

Breathing motion might cause unwanted deviations between the planned and the delivered dose distributions, resulting in a "blurred" dose distribution, with a decreased dose to the edge of the tumour and an increased dose to the surrounding healthy tissue [2]. For dynamic treatment techniques, such as VMAT and proton pencil beam scanning (PBS), the simultaneous movement of the treatment delivery and the tumour may, in addition, cause interplay effects, which are difficult to predict and result in an unwanted heterogeneous dose distribution [2]. Although these dose heterogeneities average out when multiple treatment fractions are delivered [2-8], the biological consequences of delivering a heterogeneous dose distribution at each fraction are not well known. Dose blurring can be accounted for by increasing the treatment margins. However, increasing the treatment margins increases the dose to the surrounding healthy tissue and hence the risk of side effects and does not adequately account for interplay effects. Different motion mitigation techniques, such as respiratory gating, breath-hold and real-time tumour tracking, could be used to minimise both the healthy tissue dose and interplay effects [1, 9]. In addition to mitigating motion, respiratory gating and breath-hold performed during deep inspiration (DI) might lead to favourable anatomical changes in the position of the tumour with respect to healthy tissue and to decreased lung density.

These changes may result in a reduced dose to healthy tissue, which could be beneficial in the treatment of breast cancer, lung cancer, liver cancer and mediastinal lymphomas [9, 10].

With the current refined radiotherapy techniques, it is important to know the dosimetric effects of breathing motion. Knowledge of the potential benefits and disadvantages of breathing motion enables individualized optimisation of the radiotherapy treatment for each patient. Thus, the potential benefits of DI combined with different delivery techniques need to be investigated for various diagnoses. The possible introduction of additional uncertainties, such as variations in the DI level, should be considered. Motion mitigation techniques are not always clinically feasible, so moving tumours are often treated during free breathing (FB). Thus, interplay effects might pose a problem, but determining the dosimetric effects of interplay is particularly challenging because of their unpredictable nature. No current commercial system explicitly accounts for interplay effects in the treatment planning process.

Aims

The overall aim of the work presented in this thesis was to investigate the dosimetric effects of breathing motion in radiotherapy.

The first goal was to investigate the dosimetric effects of DI during both photon and proton therapy. The specific goals were to investigate

- potential healthy tissue dose sparing using DI during photon or proton therapy for left-sided breast cancer,
- intrafractional DI reproducibility for left-sided breast cancer and the resulting dosimetric effect on the target and healthy tissue, and
- potential healthy tissue dose sparing using DI during photon or proton therapy for mediastinal Hodgkin's lymphoma (HL).

The second goal was to investigate breathing-motion-induced interplay effects in VMAT treatment. The specific goals were to

- develop a tool to simulate motion-induced interplay effects for VMAT,
- investigate how motion-induced interplay effects vary with different patient- and machine-specific parameters, and
- investigate the impact of motion-induced interplay effects for VMAT in a clinical setting.

Background

In radiotherapy, the most optimal treatment plan is sought for each individual patient, whereby a high dose is given to the tumour while minimising the dose to the surrounding healthy tissue. To achieve this goal, images of the patient are first acquired, usually using computed tomography (CT), in which target volumes (TVs) and organs at risk (OARs) are delineated [11-13]. The gross tumour volume (GTV) contains the visible and/or palpable tumour and the clinical target volume (CTV) contains the GTV and/or the subclinical microscopic disease. To account for different uncertainties, margins are added to the CTV to create the planning target volume (PTV). The CTV-to-PTV margin is divided into internal and setup margins. The internal margin accounts for variations in the position, size, and shape of the CTV due to motion, creating the internal target volume (ITV), and the setup margin accounts for patient positioning as well as dosimetric and mechanical uncertainties. A treatment plan is then created in a computer-based treatment planning system (TPS), using one of several possible treatment techniques.

Treatment techniques

In radiotherapy, several different techniques can be used to treat the patient. The most common is photon therapy using high-energy X-rays, but the use of proton therapy has increased rapidly in the last few years [14].

Photon therapy

The high-energy photons used in radiotherapy are produced by a linear accelerator (linac). In the linac, electrons are accelerated and then hit a high-density target, upon which photons are generated by the bremsstrahlung production process. The produced photon beam is forward-peaked, so to generate a uniform beam, a cone-shaped flattening filter is used. The beam is shaped using collimators, which create rectangular fields of different sizes. The beam can be further conformed to the TV by using multileaf collimators (MLC), consisting of several “leaves”, which can be individually positioned to shield surrounding healthy tissue and moved to modulate

the intensity of the beam. These components are mounted on a gantry that can rotate 360° around the patient, allowing irradiation from different angles.

Various photon therapy techniques are available, such as three-dimensional conformal radiotherapy (3D-CRT) **(papers I-IV)**, intensity modulated radiotherapy (IMRT) [15], and VMAT [16, 17] **(papers IV-VI)**. For small TVs such as early-stage tumours or small metastases, stereotactic body radiotherapy (SBRT) is often used, where an ablative dose of radiation (typically 15-20 Gy) is given in few fractions (**paper VI**) [18, 19]. For IMRT, VMAT, and SBRT, a uniform beam is not necessary and the flattening filter can be removed, generating so-called flattening-filter free (FFF) beams (**papers V and VI**) [20]. This allows a higher dose rate to be used, which, in some cases, shortens the delivery time [21].

3D-CRT

A 3D-CRT plan consists of static beams that are shaped by the MLC to conform to the TV. This technique is forward-planned, which can be described as a trial-and-error process where parameters such as energy, angle, shape, and weight are manually adjusted for each beam until the desired dose distribution is achieved. Usually, several beams from different directions are used to provide a high dose to the TV and a low dose to the surrounding healthy tissue.

IMRT and VMAT

So-called inverse treatment planning is used for IMRT and VMAT, where objectives with different priorities are assigned to TVs and OARs. The beam intensities are adjusted to fulfil these objectives by using an iterative optimisation process that finds the global minimal difference between the calculated and optimal dose distributions. This process produces beams of varying intensities, as opposed to 3D-CRT, where the intensity of each beam is uniform. The nonuniform intensities are realised at the linac by delivering the radiation in smaller segments shaped by the MLC. For IMRT, several fixed gantry angles are used, whereas for VMAT, the radiation is delivered while the gantry is continuously rotating around the patient, enabling shorter delivery times [17, 22]. For VMAT, the position of the collimators and the MLC, the gantry speed, and the dose rate vary continuously during radiation delivery. These parameters are specified at discrete, so-called control points that are at a fixed angular interval, and linearity between the control points is assumed. Both IMRT and VMAT provide a very conformal high-dose distribution, especially for concave and complex TVs, however, at the expense of larger healthy tissue volumes receiving low doses.

Proton therapy

When protons interact with matter, they deposit the highest amount of energy per unit length close to their range, resulting in the so-called Bragg peak [23]. However, the Bragg peak is rather narrow and does not cover the extent of a tumour. To extend the high-dose region in depth, several Bragg peaks with different energies are delivered to create a spread-out Bragg peak (SOBP). The steep distal fall-off of the SOBP enables superior dose distributions compared to photon therapy techniques. While IMRT and VMAT reduce OAR volumes irradiated to high doses at the expense of larger volumes irradiated to low doses, proton therapy allows the reduction of OAR volumes irradiated to all dose levels. In proton therapy, a narrow pencil beam is generated using either a cyclotron or a synchrotron and is spread out using two different techniques: passive scattering [24, 25] and pencil beam scanning (PBS) [26, 27].

Passive scattering

In passive scattering, lateral broadening is accomplished by placing a scattering material in the beam. Patient-specific apertures shape the broadened beam to the TV outline. A range modulator is used to create a SOBP of appropriate depth by placing materials of different thicknesses in the beam for a varying amount of time. This creates a SOBP with a fixed extent in depth that is conformed to the distal part of the TV using patient-specific compensators. However, because the extent of the SOBP is fixed across the field, it is not possible to conform the dose to the TV proximally.

Pencil beam scanning

In PBS, the narrow pencil beam is scanned across the TV. Magnets are used to steer the beam in the lateral directions, and by changing the energy and intensity of the beam the dose can be delivered in "spots". The advantage of this technique is that the dose can be conformed to the TV both proximally and distally. There are two different techniques for delivering PBS: single field uniform dose (SFUD) and intensity modulated proton therapy (IMPT) [28]. For SFUD, individually optimised fields, each of which delivers a homogeneous dose across the TV, are combined. This corresponds to the use of open fields in photon therapy. For IMPT, however, all fields are simultaneously optimised, resulting in a heterogeneous dose distribution across the TV for each field. This corresponds to IMRT in photon therapy. In general, IMPT can produce more conformal dose distributions compared to SFUD, but are more sensitive to uncertainties that arise, for example, from setup errors and motion, because of the heterogeneous field dose distributions [29]. Proton PBS plans, using both IMPT and SFUD, were created in **papers II and IV**.

Relative biological effectiveness

A physical dose of protons produces a higher biological effect than does the same physical dose of photons. The relative biological effectiveness (RBE) is used to compare proton and photon dose distributions, and is defined as the ratio of the dose of reference photons to the dose of protons required to produce the same biological effect. A constant RBE of 1.1 is commonly used [30], but in reality the RBE depends on the dose per fraction, beam energy, tissue type, and position in the SOBP. The RBE increases towards the distal edge of the SOBP, resulting in an extended biological effective range of a few millimetres [31].

Motion in radiotherapy

Motion during radiotherapy is inevitable for a large number of tumour sites, and can degrade the dose distribution to the TV and the OARs [32]. Different types of motion can occur on different timescales. These motions can be categorised as setup uncertainties or organ motion, where the former is the motion of the patient as a whole relative to the radiation beam and the latter is the motion within the patient. Setup uncertainties can be minimised with the use of good immobilization devices and image guidance, whereby images (usually X-rays) are acquired before treatment delivery and matched with the patient position during the planning CT [33]. Organ motion may occur either between (interfraction) or during (intrafraction) treatment fractions. Examples of interfraction organ motion, which occurs on a day-to-day or week-to-week time scale, are differences in daily bowel- and bladder-filling, tumour shrinkage or growth, and patient weight loss or gain. Examples of intrafraction organ motion, which occurs in minutes or seconds, are breathing, heartbeat, peristalsis, swallowing, cough, and eye movement.

Dosimetric effects of breathing motion

Breathing is the dominant cause of organ motion and affects tumours in the thorax and abdomen [1, 2]. Tumour motion due to breathing has been shown to be highly patient specific with reported magnitudes of displacement of up to 3 cm and the largest displacement in the cranio-caudal (CC) direction [1, 34, 35]. The tumour follows complex trajectories and the breathing pattern might change with respect to magnitude, period, regularity, and baseline position from cycle to cycle (intrafraction) or day to day (interfraction) [34, 35]. Breathing motion might result in deviation between the planned and delivered dose distributions in the form of dose blurring, interplay effects, and range uncertainties [2, 29, 36, 37].

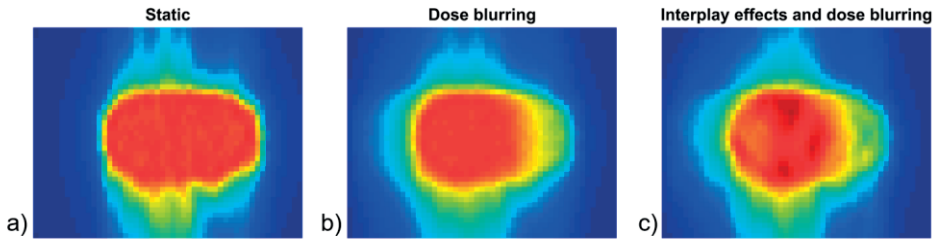

Figure 1 Examples of (a) a static dose distribution, (b) a dose distribution that includes dose blurring, and (c) a dose distribution that includes both interplay effects and dose blurring. Motion was in the left-right direction.

Dose blurring

Dose blurring occurs regardless of treatment technique and results in a widening of the penumbra, which decreases the dose at the edges of the TV and increases the dose to nearby OARs (Figure 1). This effects can be described as a convolution of the static dose distribution with the function describing the motion pattern. Because of the steep fall-off of the SOBP, dose blurring may be more severe in proton therapy than in photon therapy.

Interplay effects

In addition to dose blurring, interplay effects may occur for dynamic treatment techniques, such as IMRT, VMAT and PBS, where there is a simultaneous movement of the tumour and treatment delivery (MLC motion, gantry rotation, varying fluence and spot delivery). Interplay effects might result in a heterogeneous dose distribution with undesirable hot and cold spots (Figure 1). A schematic illustration of interplay effects between a moving tumour and the motion of the MLC in IMRT or VMAT is presented in Figure 2; the same principle applies in PBS. The dose to a certain point might vary considerably depending on the motion of the point relative to the motion of the MLC leaves. If the motion is such that the point is covered more by the MLC leaves than when it is static, the point receives a lower dose than planned. However, if the motion is such that the point is covered less by the MLC leaves than when it is static, the point receives a higher dose than planned. This results in a heterogeneous dose distribution with over- and underdosed subvolumes within the TV (Figure 1). Motion-induced interplay effects for VMAT were investigated in **papers V and VI**.

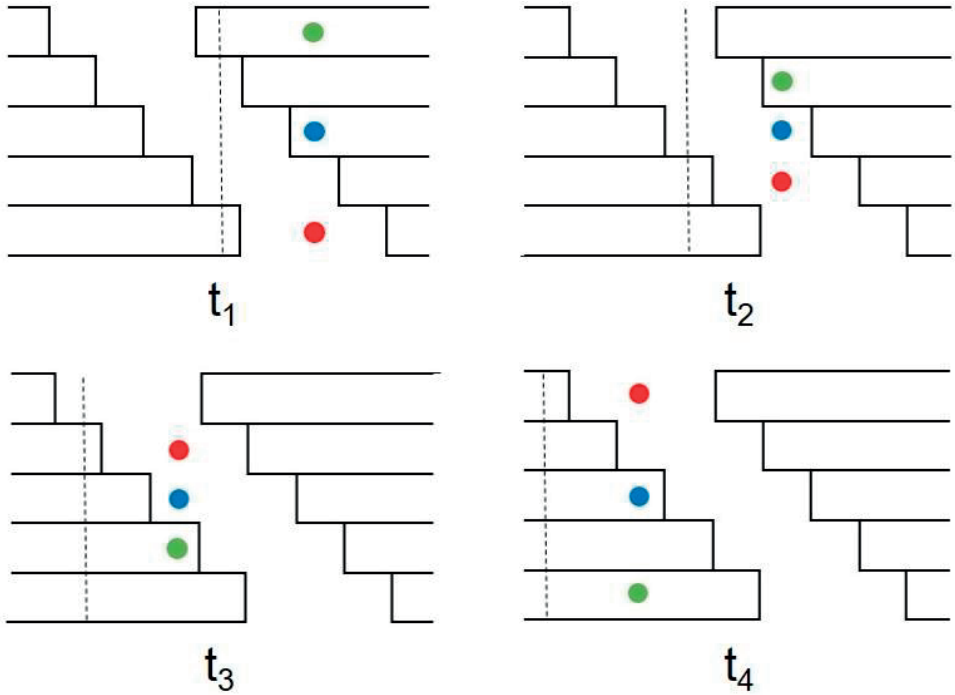

Figure 2 Schematic illustration of the interplay effects between a moving tumour and the motion of the multileaf collimator (MLC) during intensity modulated radiotherapy (IMRT) or volumetric modulated arc therapy (VMAT) for three different treatment scenarios, represented by the blue, green, and red points. For four different time points (t_1, t_2, t_3 and t_4), the MLC leaves move from left to right while the green and red points move up and down with different phases relative to the motion of the MLC. The green and red points are covered more and less by the MLC leaves compared to the static blue point, resulting in under- and overdosage, respectively.

Range uncertainties

Motion from breathing might cause the density, and hence the radiological pathlength, to change along the direction of the beam. This variation largely affects the range of the protons, resulting in a shift of the SOBP, which might lead to a large underdosing of the TV and overdosing of the OARs. However, the effects of range uncertainties have only a minor impact in photon therapy.

Motion management techniques

Different methods such as increased treatment margins, respiratory gating, breath-hold and tumour tracking can be used to mitigate the effects of breathing motion [1, 9, 10]. Increasing the treatment margins ensures target coverage despite the motion, but at the expense of irradiating larger volumes of healthy tissue. In addition, increasing the treatment margins does not account for interplay effects. The

treatment margin approach was used to account for breathing motion in **papers V and VI** and is further explained below. During respiratory gating, the patient breathes normally whereas for the breath-hold technique the patient hold his or her breath. The breathing motion is monitored so that the radiation is delivered only when the TV is in a certain position. During tumour tracking, the beam instead follows the TV continuously during radiation delivery. Performing respiratory gating and breath-hold during DI could result in a more favourable anatomical setting, with increased distance between the TV and OARs and decreased lung density. Two techniques for radiation delivery during DI are enhanced inspiration gating (EIG) and deep inspiration breath-hold (DIBH) [9, 38], which were used in **papers I-IV** and are further explained below. To some degree, fractionated treatment and the use of multiple treatment fields average out interplay effects [2-4, 6-8, 39]. In PBS, so-called rescanning, where the TV is scanned multiple times during one treatment fraction, is often used to mitigate interplay effects [37, 39].

Treatment margin approach

To determine individual ITV margins for each patient, the tumour motion must be determined before treatment. This knowledge can be obtained from a four-dimensional CT (4DCT) scan during FB (Figure 5). During acquisition of a 4DCT scan, breathing is monitored and a breathing curve is generated. Simultaneously, oversampled CT images are acquired and retrospectively sorted, on the basis of the breathing curve, creating complete time-resolved 3D images that represent different parts (usually 8-10) of the breathing cycle [40, 41]. Abdominal compression, whereby a plate is pressed against the abdomen of the patient during imaging and treatment, can be used to limit tumour motion [18].

The ITV can then be created as the union of the CTVs from all phases in the 4DCT scan. To facilitate the delineation of the ITV, the maximum intensity projection, which is a reconstructed CT image in which each voxel contains the maximum intensity of all the phases of the 4DCT scan, can be used [42]. Another method to determine treatment margins is to calculate the time-weighted mean position of the tumour based on the 4DCT images, the so-called mid-position [43]. In the mid-ventilation approach, the structure delineation, treatment margin generation, and dose calculation are based on the phase in the 4DCT image closest to the mid-position (**paper VI**) [44].

EIG and DIBH

During EIG, the patient breathes deeply continuously, with inhale and exhale times of approximately 4-5 s, whereas for DIBH, the patient performs deep breath-holds for a longer period of time (approximately 15-30 s) and breathes normally in between them (Figure 3) [9, 38]. During EIG and DIBH, imaging and treatment delivery are performed only during DI, when the breathing curve is within a preset

gating window (Figure 3). Treatment is often delivered during multiple breath-holds, so it is important that the inspiration level is stable during each breath-hold and is reproducible from one breath-hold to another. The use of visual guidance, where the patient can follow his or her breathing projected on a screen or using video goggles in real-time, has been shown to improve intra-breath-hold stability and inter-breath-hold reproducibility [45, 46]. Visual guidance is often used in combination with audio guidance, where the patient is verbally instructed when to breathe in and out.

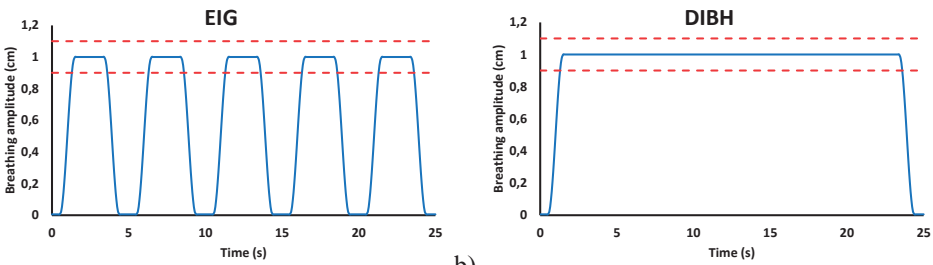

a) b)

Figure 3 Schematic breathing curves (solid blue lines) for the two deep inspiration techniques: (a) enhanced inspiration gating (EIG) and (b) deep inspiration breath-hold (DIBH). Radiation is delivered only when the breathing curve is within the gating window (dashed red lines).

Motion monitoring

During both EIG and DIBH, as well as during 4DCT acquisition, breathing needs to be monitored to synchronise the treatment delivery or imaging with the breathing, which generate so-called breathing curves (Figure 3). Breathing motion can be monitored using direct visualization of the tumour or internal fiducial markers, for example, with continuous X-ray imaging [1, 10]. However, direct visualization is often difficult, so the breathing curve usually is obtained from an external surrogate such as the motion of the chest wall, which is assumed to correlate with the TV motion [9]. Surrogate systems for monitoring breathing motion include a marker block [real-time position management (RPM) system, Varian Medical Systems, Palo Alto, CA, USA], spirometer [Active Breathing Coordinator (ABC), Elekta AB, Stockholm, Sweden], pressure sensor (Anzai, Siemens Medical Systems, Concord, CA, USA), and optical surface scanning (OS) systems (Sentinel and Catalyst, C-rad, Uppsala, Sweden, and AlignRT, VisionRT, London, UK). The RPM system or the Sentinel and Catalyst systems were used to monitor breathing during EIG and DIBH in **papers I-IV**, and the Anzai pressure sensor was used during 4DCT acquisition in **paper VI**.

The RPM system consists of a marker block with six reflective markers, and is placed on the chest wall of the patient. The anterior-posterior (AP) movement of the block is monitored using infrared light, which is reflected by the markers and

detected by a camera. The OS systems Sentinel and Catalyst reconstruct a 3D surface of the patient (Figure 4) using laser scanning and projection of visible light, respectively, and can be used for patient positioning, motion monitoring during treatment delivery, and to trigger radiation delivery during DIBH [47-49]. The Sentinel system is used during CT scanning and the Catalyst system during treatment. The advantage of OS systems is that they are deviceless systems that monitor the whole surface of the patient without contributing any (imaging) radiation dose. In addition, the isocenter position can be determined in real time based on the surface information using a nonrigid registration algorithm [50, 51]. This method was used in **paper III** to determine the intrafractional DIBH reproducibility. The Anzai system consists of an elastic belt with a pressure sensor that is placed around the abdomen of the patient. The sensor monitors breathing in real time because the pressure increases during inspiration and decreases during expiration [52].

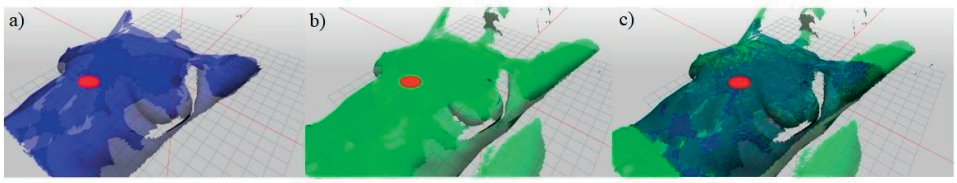

Figure 4 Example of (a) a reference surface and (b) a real-time live surface obtained by the optical surface scanning system Catalyst during a deep inspiration breath-hold (DIBH) treatment for left-sided breast cancer. (c) Treatment delivery is triggered when the surfaces within the red circle coincide. Adopted from **paper III**.

Time-resolved dose calculation using deformable image registration

Image registration can register images from different modalities [such as CT, magnetic resonance imaging (MRI), and positron emission tomography (PET)] or time series (such as 4DCT) to aid in the delineation of TVs and OARs or for dose accumulation. The purpose of image registration is to find the geometrical transformation that maps one image (moving image) onto another (fixed image) [53, 54]. An optimisation strategy iteratively changes the transformation until an optimal value of a similarity metric that corresponds to the best alignment of the two images is obtained. A registration is perfect when the transformed image is identical to the fixed image. Usually, a rigid transformation, which accounts for translations and rotations, is used. However, deformations due to anatomical changes such as breathing may occur, requiring deformable image registration (DIR) algorithms. The use of DIR results in a transformed image with an associated deformation vector field (DVF) that describes the motion from the moving to the fixed image for each individual voxel (Figure 5).

The use of DIR allows the accumulation of dose from several different time points into a common geometry [55, 56]. This characteristic could be used to determine

the dosimetric impact of breathing motion by using DIR to register different phases of a 4DCT scan (Figure 5). The resulting DVFs could then be used to accumulate the dose from the different phases into one common reference phase. This dynamic dose accumulation method was used to determine the dosimetric impact of breathing-motion-induced interplay effects for VMAT in **paper VI**.

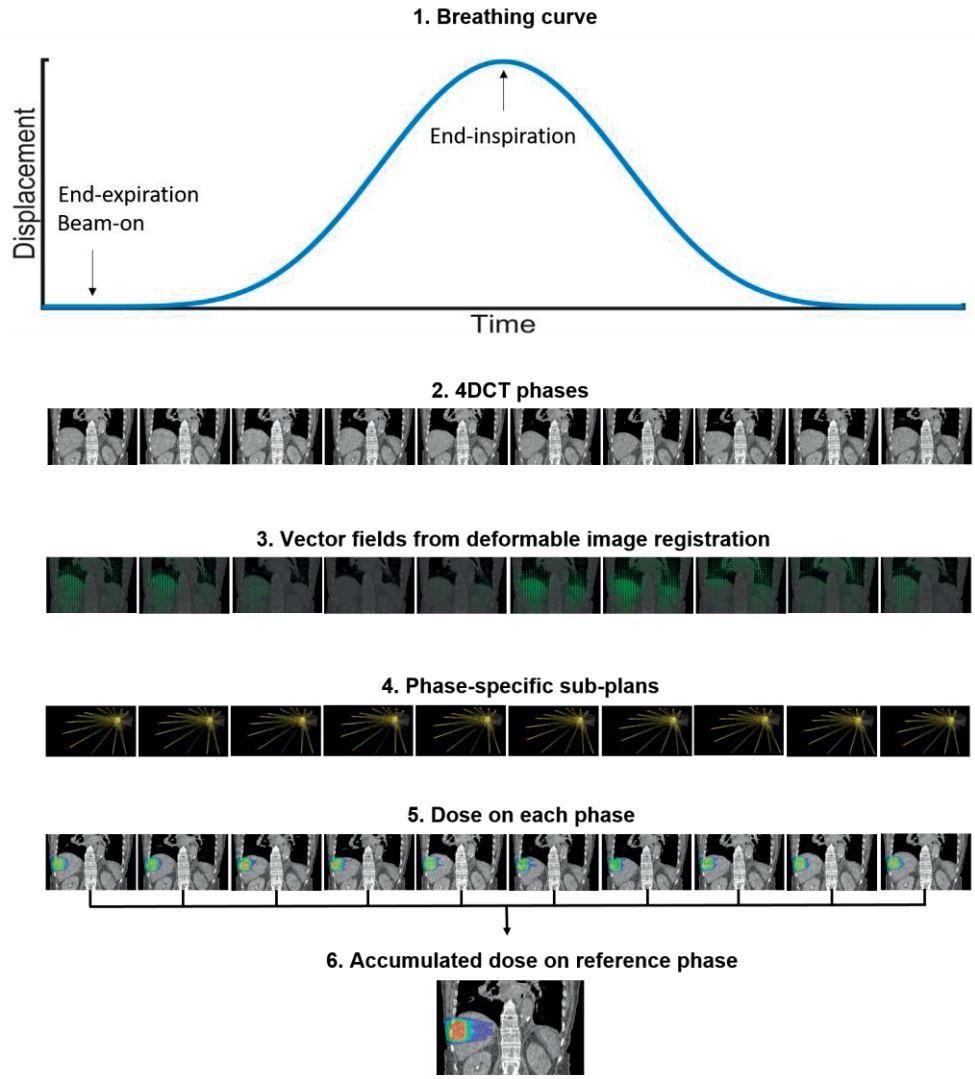

Figure 5 Schematic illustration of time-resolved dose calculation based on deformable image registration (DIR). Based on a breathing curve (1), four-dimensional computed tomography (4DCT) images are acquired (2), where each phase corresponds to a specific part of the breathing curve. Deformation vector fields (DVFs) that describe the motion of each voxel in the different 4DCT phases relative to a reference phase are obtained using DIR (3). A treatment plan is divided into phase-specific sub-plans (4), which are calculated on the corresponding phase of the 4DCT (5). The total dose is accumulated on the reference phase based on the DVFs (6). Adopted from **paper VI**.

Evaluation techniques

To evaluate and compare dose distributions, various dosimetric analysis methods and statistical tests can be used. Usually, the dose distributions are evaluated, but ultimately it is the clinical outcome of the treatment that is important. Therefore, it is of interest to find the probabilities of the occurrence of certain endpoints: the tumour control probability (TCP) and the normal tissue complication probability (NTCP).

Dosimetric analysis

Dose distributions are usually evaluated using differential and cumulative dose-volume histograms (DVHs), which display the volume of the target or the OAR that receives a dose equal to and greater than or equal to a certain value, respectively. From the DVHs, different dosimetric parameters can be retrieved, such as the minimum, maximum, and mean dose (D_{mean}), the volume that receives a dose ≥ X%/Gy ($V_{X\%/Gy}$), and the dose to Y%/cm^3 of the volume ($D_{Y\%/cm3}$). Furthermore, the heterogeneity index (HI) can be calculated as (**papers II, IV, and VI**)

$$HI = \frac{D_{2\%} - D_{98\%}}{D_{mean}} \quad (1)$$

where $D_{2\%}$ is the dose to 2% of the volume (near maximum dose) and $D_{98\%}$ is the dose to 98% of the volume (near minimum dose). The integral dose (ID) determines the total amount of energy delivered to healthy tissue and can be calculated as (**papers II and IV**)

$$ID = \rho \cdot V \cdot D_{mean} \quad (2)$$

where ρ is the density and V the structure volume. An example of the different conformity indices that are used to indicate how well the high-dose distribution conforms to the TV [57] is Paddick's conformity index ($CI_{Paddick}$) [58], which is calculated as (**paper IV**)

$$CI_{Paddick} = \frac{TV_{PIV}^2}{TV \cdot PIV} \quad (3)$$

where PIV the prescription isodose volume and TV_{PIV} is the TV covered by the PIV.

Statistical analysis

Different statistical tests can be used to investigate whether there is a "real" difference in a dosimetric parameter between two or more treatment techniques, or if the difference only occurred by chance [59]. These tests are either parametric or non-parametric. Parametric tests require that certain assumptions about the data be fulfilled. The data have to be normally distributed and, in case of unpaired data,

have similar variance between the groups. Otherwise, non-parametric tests must be used. In this thesis, the following statistical tests were used:

- Student's t-test (**paper II**)
- Wilcoxon test (**papers I, III, IV, and VI**)
- Friedman test (**papers IV and VI**)

Only paired tests were used, because different treatment techniques were always compared for the same patient material. Student's t-test is a parametric test that compares two techniques. The Wilcoxon test is the corresponding non-parametric test for paired data. If more than two techniques are being compared, an omnibus test is first conducted to find if there is an overall difference between any of the techniques. An ANOVA test can be used for parametric data and a Friedman test can be used for non-parametric data. If an overall difference is found, multiple paired tests are performed to find the techniques between which there is a statistically significant difference. When performing multiple comparisons, the probability of detecting a statistically significant difference increases when in fact there is no difference. One way to account for this is to perform a Bonferroni correction, where the significance level is divided by the number of comparisons.

TCP and NTCP

The probability of the occurrence of a certain endpoint as a function of the dose and irradiated volume of the target and OARs can be described by TPC and NTCP models, respectively, which are often S-shaped sigmoid functions [60]. The best fit of the model parameters to a known data set for a large number of patients is determined. The data set consists of the clinical outcomes for a specific endpoint and the corresponding dose distributions (most commonly DVHs). Using these parameters and the shape of the model, the TCP and NTCP for other patient cohorts can be predicted. Two commonly used NTCP models are the Lyman-Kutcher-Burman (LKB) model [61] and the relative seriality model [62]. In **paper I,** the relative seriality model [Eqs. (4) and (5)] was used to estimate cardiac mortality and radiation pneumonitis following breast cancer radiotherapy.

$$\mathrm{NTCP} = \{1 - \prod_{i=1}^{n}[1 - \mathrm{P}(D_i)^s]^{\Delta V_i}\}^{1/s}, \quad (4)$$

$$\mathrm{P}(D_i) = 2^{-\exp\{e\gamma(1-D_i/D_{50})\}}, \quad (5)$$

where D_i is the absorbed dose in each dose bin i of the differential DVH, D_{50} is the dose that results in 50% complication probability, γ is the maximum relative slope of the dose-response curve, n is the number of DVH dose bins, and $\Delta V_i = V_i/V$, where V_i is the volume of each dose bin i and V is the total volume of the organ. The relative seriality factor s (range 0 to 1) describes the volume dependence.

Deep inspiration photon or proton therapy

Both breast cancer and HL patients have favourable prognoses and a long life expectancy, and may risk developing late effects from radiotherapy. Thus, it is important to minimise the dose to healthy tissue for these patients as much as possible. A promising method to achieve this is to perform the treatment during DI [9, 10]. Because the TV is either attached to the chest wall or in the mediastinum for these patients, there is a good correlation between the motion of the TV and chest wall that allows the use of external surrogates for motion monitoring [63]. In the work presented in this thesis, potential healthy tissue sparing using DI during photon or proton therapy was investigated for both left-sided breast cancer (**papers I-III**) and mediastinal HL (**paper IV**).

Left-sided breast cancer

The use of adjuvant radiotherapy to treat breast cancer has been shown to reduce the risk of local and locoregional recurrence as well as death from breast cancer [64, 65]. However, radiotherapy has also been associated with an increased risk of cardiovascular and pulmonary diseases [66-79]. A higher incidence of coronary artery disease has been observed in left-sided versus right-sided breast cancer patients. The left anterior descending coronary artery (LAD) is especially exposed to high doses because of its location in the anterior part of the heart, often within the treatment fields (Figure 6) [74, 79]. Darby et al. [69] showed that the relative risk of ischaemic heart disease increased with the increase in the D_{mean} to the heart by 7.4%/Gy, with no apparent threshold. This was recently validated by van den Bogaard et al. [72] for more modern radiotherapy techniques. Thus, any reduction in the heart dose would be beneficial to the patient, so it is important to keep it as low as possible. Of the many methods proposed to reduce the heart dose [80], treatment during DI [63, 81-84] and proton therapy [85-93] have shown great potential. In addition, the use of these two techniques combined has been investigated [94-97]. The potential healthy tissue sparing using DI during photon therapy for left-sided breast cancer was investigated in **papers I and III**, and the

additional benefit of using proton therapy in combination with DI was investigated in **paper II**. Those papers presented pure treatment planning studies. However, it is of utmost importance that any potential dosimetric benefit of DI is maintained during treatment delivery. This requires that the DI technique used be reproducible and stable [83]. Therefore, the dosimetric effects of intrafractional DIBH reproducibility were investigated in **paper III**.

Comparison of deep inspiration and free breathing

In **paper I**, 32 patients who had been treated with adjuvant radiotherapy for left-sided breast cancer were retrospectively enrolled in the study. Sixteen patients had received tangential treatment (to the breast only) after breast-conserving surgery and 16 patients had received locoregional treatment (including the axillary lymph nodes and supra- and infraclavicular fossa) after either breast-conserving surgery or mastectomy. CT images during both audio-coached EIG and FB were acquired for all patients. The RPM system was used to monitor breathing and to automatically trigger imaging and treatment delivery. The median breathing amplitude was 7.0 mm for tangential treatment and 6.9 mm for locoregional treatment.

In **paper III**, 40 patients who had been treated with adjuvant radiotherapy for left-sided breast cancer were retrospectively enrolled in the study. Twenty patients received tangential treatment after breast-conserving surgery and 20 patients received locoregional treatment after either breast-conserving surgery or mastectomy. CT images during both visual- and audio-guided DIBH and FB were acquired for all patients. Optical surface scanning was used to monitor breathing and trigger the irradiation during CT and treatment delivery, respectively. The median breathing amplitude was 10.5 mm for tangential treatment and 10.3 mm for locoregional treatment.

In both **papers I and III**, TVs and OARs (CTV-T, PTV, heart, LAD, and ipsilateral lung) were delineated in both the DI (EIG and DIBH) and FB CT images. Essentially identical 3D-CRT plans were created for DI and FB, based on national guidelines (www.swebcg.se). The OAR doses were kept as low as possible, but the target coverage was always prioritized higher than the OAR doses to ensure a fair comparison between the different techniques. The prescribed dose was 50 Gy in 25 fractions. The treatment plans were created using the Eclipse TPS (Varian Medical Systems, Palo Alto, CA, USA) and were calculated using the anisotropic analytical algorithm (AAA). DVHs were retrieved from the TPS and different dosimetric parameters were compared. Two-sided paired Wilcoxon tests were performed to see if the differences between DI and FB were statistically significant.

Healthy tissue dose sparing

Treatment during DI led to favourable anatomical changes, with an increased distance between the heart and breast and decreased lung density (Figure 6). **Papers I and III** showed that for both tangential and locoregional treatment, doses to the heart and LAD were significantly reduced for comparable target coverage during DI compared to FB (Figure 7). In **paper III**, the ipsilateral lung dose was significantly reduced using DIBH for both tangential and locoregional treatment, whereas in **paper I** the lung dose was reduced for only locoregional treatment using EIG, with no significant difference observed for tangential treatment.

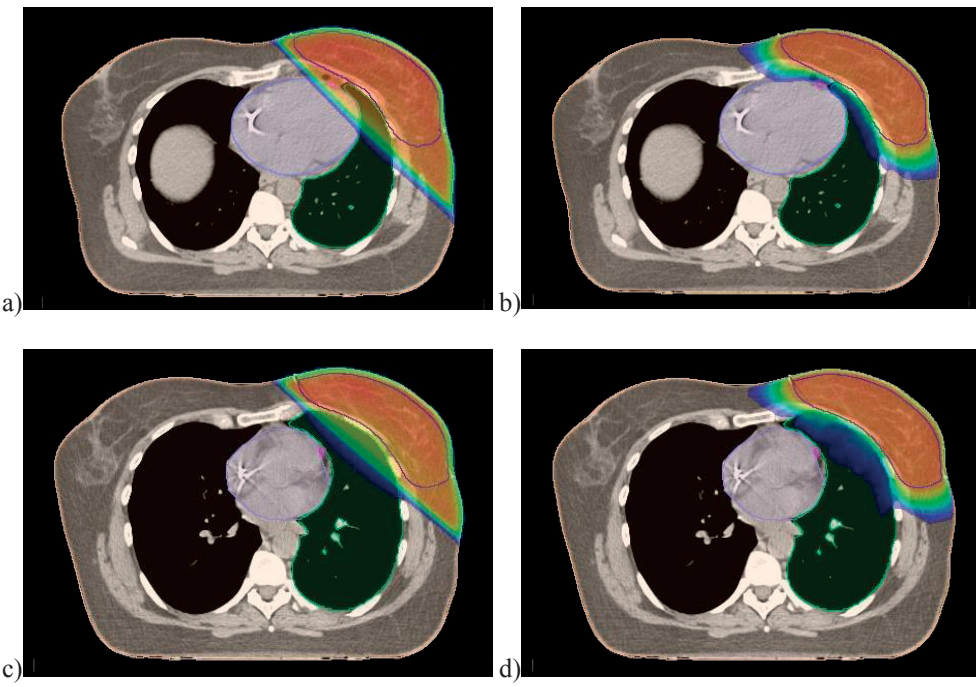

Figure 6 Transversal dose distributions (15% to maximum dose) for one left-sided breast cancer patient in **papers I and II** for (a) free breathing (FB) photon, (b) FB proton, (c) enhanced inspiration gating (EIG) photon, and (d) EIG proton therapy. The planning target volume (PTV) is outlined in blue, the heart is outlined in purple, the left anterior descending coronary artery (LAD) is outlined in pink, and the ipsilateral lung is outlined in green.

The OAR dose reductions in **papers I and III** are comparable to the dose reductions observed in previous studies [81-83] and may lead to reduced long-term risk of mortality and morbidity due to cardiovascular and pulmonary diseases. The dose was calculated using the AAA, as opposed to the previously widely used pencil beam algorithm accounts for lateral electron transport. Use of AAA results in a more accurate dose calculation in low-density volumes such as the lung [98, 99]. **Paper I** showed that although EIG reduced the dose to the heart and LAD, the heart was completely outside the treatment fields for only a small proportion of patients (38%

for tangential treatment and 25% for locoregional treatment). Complete elimination of the heart and LAD from the treatment fields, and, hence, from exposure to high doses, could be clinically important [79, 100, 101]. The breathing amplitudes in **paper I** could be considered rather low and Damkjær et al. [38] showed that larger amplitudes could be achieved with visually guided DIBH than with audio-coached EIG. This was confirmed by Bergh [45], who also showed improved reproducibility and stability for visually guided DIBH compared to audio-coached EIG. Therefore, DIBH with visual guidance, monitored using OS, was clinically implemented at Skåne University Hospital in 2015, replacing audio-coached EIG, which had been in clinical use since 2007.

In **paper III**, larger breathing amplitudes were achieved using visually guided DIBH, resulting in the heart being completely outside the treatment fields in a larger proportion of patients (80% for tangential treatment and 45% for locoregional treatment). It is difficult to compare the dosimetric benefits observed in **papers I and III**, because of different patient cohorts and variations in the structure delineations and treatment plans. However, the relative heart and LAD dose reductions observed in **paper I** were slightly larger than those in **paper III**, probably because of the higher absolute OAR doses in **paper I**. The lung dose was significantly reduced for tangential treatment using DIBH in **paper III,** but this reduction was not observed with the use of EIG in **paper I.** Similar results were obtained by Damkjær et al. [38], probably because of the larger breathing amplitudes achieved using DIBH and visual guidance.

According to both **papers I and III**, treatment during DI was more beneficial for locoregional than for tangential treatment because of the larger OAR doses for locoregional treatment. The internal mammary nodes (IMN) were not included in the TV, which was the clinical practice when the studies were conducted. The use of DI is more important when the IMNs are included in the TV, because their inclusion results in higher OAR doses and, thus, potentially greater OAR dose sparing [81-83]. The largest uncertainty in **papers I and III** is probably the difference between the structure delineations of DI and FB, especially those for LAD because of its small volume. Comparable structure volumes and target coverage are crucial for a fair comparison of the OAR doses of the different treatment techniques. To reduce the interobserver variations, the same oncologist delineated all the structures and the same dosimetrist/physicist created the treatment plans for both DI and FB in each treatment planning study (**papers I-IV**).

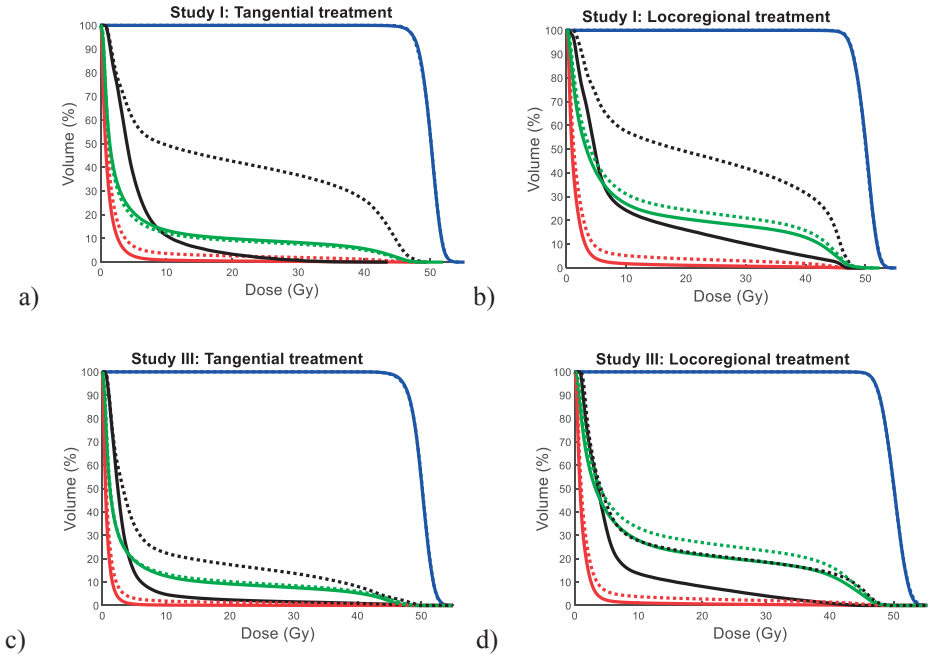

Figure 7 Average dose-volume histograms for (a,c) tangential and (b,d) locoregional photon therapy of left-sided breast cancer, comparing doses to the heart (red), left anterior descending coronary artery (black), ipsilateral lung (green), and planning target volume (blue) using deep inspiration (solid lines) and free breathing (dashed lines). Adopted from **papers I and III**.

NTCP

To investigate whether the OAR dose reductions observed in **paper I** using EIG is expected to translate into reduced risk of late effects, NTCP calculations were performed for the two endpoints excess cardiac mortality and radiation pneumonitis using the relative seriality model [Eqs. (4) and (5)]. Input parameters derived by Gagliardi et al. [101, 102], and corrected for the use of the AAA for radiation pneumonitis according to Hedin et al. [103], were used.

The results of the NCTP calculations reflected the dose differences observed. The excess cardiac mortality probability was reduced with the use of EIG compared to FB for both tangential and locoregional treatment. The risk of radiation pneumonitis was reduced with the use of EIG for locoregional treatment, but no significant difference in risk was observed for tangential treatment. There are several uncertainties in the NTCP calculations, so the results should be seen as a relative comparison between EIG and FB rather than focusing on the absolute values. The NTCP parameters used were based on older radiotherapy techniques, which resulted in higher complication probabilities than estimated in **paper I**. In addition, a different dose calculation algorithm was used in **paper I** than was used to derive the

NTCP parameters, although this difference was corrected for in the radiation pneumonitis calculations, as previously mentioned.

DIBH reproducibility

In **papers I and III**, we showed that treatment during DI reduces OAR doses while maintaining target coverage. However, it is important not to introduce any uncertainties so that this benefit is maintained when the treatment is delivered to the patient. One example of uncertainty is inter-breath-hold variations within the same treatment fraction. **Paper III** also investigated the dosimetric impact of intrafractional DIBH reproducibility.

In **paper III**, OS was used to monitor breathing motion during DIBH treatment whereon beam-on was triggered by a region of interest on the skin surface above the xiphoid process (Figure 4). Visual guidance, together with a 3-mm gating window, was used to achieve reproducible DIBHs. The OS system also allowed for simultaneous real-time tracking of the isocenter position, which made it possible to investigate the reproducibility of the TV position from one DIBH to another, assuming that the isocenter position corresponds to the position of the TV. For each fraction, a reference surface was acquired the first time the patient breathed into the gating window. The live surface obtained during the rest of the treatment fraction was matched with the reference surface, and the isocenter position relative to the reference position (not including residual daily setup deviations) was obtained (Figure 4). The intrafractional DIBH isocenter reproducibility was then calculated as the difference between the average isocenter position during beam-on for two DIBHs within one treatment fraction. A total of 195 DIBHs per treatment group were analysed. The intrafractional DIBH isocenter reproducibility in the CC, AP, and left-right (LR) directions, corresponding to a cumulative probability of 50% and 90% of the DIBHs as well as the maximum values, were calculated. These values were then used to estimate the dosimetric effects on the TV and OARs by performing the corresponding isocenter shifts for the original DIBH treatment plans in the TPS.

Overall, the xiphoid process was a good surrogate for the TV during DIBH. The intrafractional DIBH isocenter reproducibility was within 1 mm for 50% of the treatment fractions and within 2-3 mm for 90% of the treatment fractions in all three directions for both tangential and locoregional treatment. These values were in accordance with the findings of previous studies [104-106]. For a few treatment fractions, intrafractional DIBH isocenter reproducibility was up to 5 mm, which resulted in large effects on the target coverage and OAR doses (Figure 8). However, in most cases, the OAR doses were still lower than with FB. Hence, despite allowing beam-on within only a 3-mm gating window based on the movement of the skin surface above the xiphoid process, larger differences in the isocenter position between DIBHs were observed. This suggests that the motion of the TV sometimes

differs from that of the xiphoid process. Therefore, it is important to not only perform DIBH based on the motion of the xiphoid process, but also set tolerance levels on the isocenter position. This can be done with the Catalyst system, thereby avoiding large isocenter deviations and the associated negative dosimetric effects.

A limitation of **paper III** is that the isocenters were shifted in the TPS assuming a rigid motion of the whole patient. This assumption implies that the distance between the TV and OARs is constant, when, in reality, it varies because breathing is a nonrigid motion. The use of DIR could have yielded results that were more accurate. However, this would have required 3D images acquired during treatment, which was not available. In addition, the same isocenter shift was assumed for all treatment fractions. However, in reality, the isocenter shift varies for each DIBH throughout the treatment, resulting in a blurring of the dosimetric effect. Finally, the isocenter shifts performed in the TPS represented the DIBH reproducibility of the entire patient cohort (50% and 90% cumulative probabilities and maximum value), and the individual DIBH reproducibility of each patient was not simulated. Hence, the dosimetric effects of DIBH reproducibility presented in **paper III** represent worst-case scenarios; the total effect for an actual treatment would be smaller.

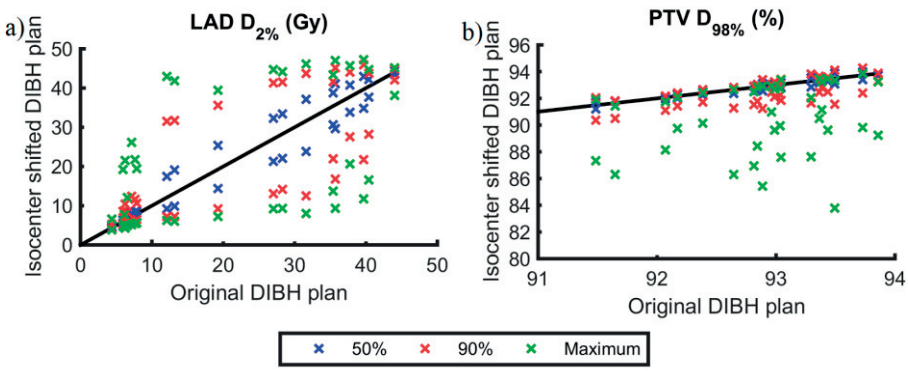

Figure 8 Dosimetric effects of intrafractional deep inspiration breath-hold (DIBH) isocenter reproducibility.The minimum and maximum values of (a) $D_{2\%}$ for the left anterior descending coronary artery (LAD) and (b) $D_{98\%}$ for the planning target volume (PTV), for the isocenter-shifted versus the original DIBH plans. The results presented are for each patient who received locoregional treatment and for three cumulative probability levels (50%, 90%, and maximum). The lines indicate where the dosimetric parameters for the isocenter-shifted and original DIBH plans are equal. The corresponding figures for all dosimetric parameters investigated, for both locoregional and tangential treatment, are presented in **paper III**.

Comparison of proton and photon therapy

Paper II investigated the additional benefit of proton therapy compared to photon therapy for left-sided breast cancer during both FB and EIG. A subset of the patient cohort in **paper I**, consisting of 10 tangential and 10 locoregional patients, formed the cohort studied in **paper II**. The same CT-images (for both EIG and FB), structure delineations, and photon plans used in **paper I** were used in **paper II**. In addition, PBS plans using both IMPT and SFUD were created for a prescribed dose of 50 Gy(RBE) in 25 fractions (using a constant RBE of 1.1). Different dosimetric parameters were retrieved from the DVHs and the HI was calculated for the PTV using Eq. (1). To compare the dose to healthy tissue of the proton plans and the photon plans, the ID was calculated using Eq. (2). The ID was calculated for the whole CT scanned body volume minus the PTV ($\rho = 1.06$ g/cm^3) and corrected for the lung density ($\rho = 0.26$ g/cm^3). Two-sided paired Student's t-tests were performed to investigate if the differences between the treatment techniques were statistically significant.

Examples of proton dose distributions, during both EIG and FB, for one patient in **paper II** are presented in Figure 6. According to **paper II**, the heart and LAD doses were reduced for proton therapy with both EIG and FB beyond what could be achieved for photon therapy with EIG (Figure 9). For locoregional treatment, proton therapy reduced the ipsilateral lung dose compared to photon therapy with both EIG and FB. For tangential treatment, however, there was no significant difference between the lung D_{mean}, but the volumes that received high and low doses were decreased and increased, respectively, for proton therapy compared to photon therapy, as indicated by the crossing of the DVHs in Figure 9g. This difference was probably due to the different field settings used for the proton and photon plans (*en face* for protons and tangential for photons). The target coverage and HI were improved with proton therapy compared to photon therapy (Figure 9a and b). In addition, the reduced ID with proton therapy, particularly for locoregional treatment, could be expected to reduce the risk of secondary cancer [107]. These results are in accordance with those of previous studies [85-96]. The differences between SFUD and IMPT were generally small.

The OAR dose reductions were larger for locoregional than for tangential treatment because larger volumes were irradiated. This result agreed with that of Ares et al. [88], who showed that proton therapy had greater benefits for more complex TVs. Thus, greater benefits can be expected if the IMNs are included in the TV. However, irradiating the IMNs is controversial, because of their proximity to the heart, and thus the increased risk of cardiotoxiciy [108, 109]. We have shown that with proton therapy, the IMNs can be included in the TV without an increase in the heart dose and with only a small increase in the ipsilateral lung dose, irrespective of whether EIG or FB is used [110].

For tangential treatment using EIG, only small differences in the OAR doses were observed between proton and photon therapy (Figure 9). In addition, the OAR dose sparing with EIG was much smaller for protons than for photons (Figure 9). Hence, the additional benefit of DI treatment in proton therapy of left-sided breast cancer is small. Treatment during DI could also mitigate breathing motion, which is generally more important in proton therapy than in photon therapy. The effects of breathing motion in proton therapy of breast cancer have been shown to be quite small and claimed not to be clinically important [88, 91, 93, 111]. However, most of these studies did not consider interplay effects, because they argued that the motion is mostly parallel to the beam direction (AP), which limit the interplay effects [111]. Because there could be large motion from breathing in the CC direction, a more thorough investigation of the impact of interplay effects in proton PBS of breast cancer is desirable. In **paper II**, a constant RBE of 1.1 was assumed; however, the RBE has been shown to increase towards the distal edge of the SOBP [31]. For breast cancer, this increase in the RBE could increase the biological effective dose to the OARs because they are situated beyond the distal edge of the SOBP. However, a variable RBE has been shown to have only a small impact due to the low OAR doses [91].

In most cases, photon therapy during DI will reduce the OAR doses to sufficiently low levels, but for selected patients, proton therapy should be considered. Proton therapy could be an alternative for patients with complex TVs that include the IMNs, patients with coexisting cardiopulmonary morbidities, and patients who do not comply with DI techniques, or when the desired separation between the TV and the OARs is not achieved using DI. Although models predict that DI and proton therapy reduce long-term cardiopulmonary mortality or morbidity [84, 94], there currently is no clinical evidence of it. Therefore, a large randomized trial (RADCOMP, ClinicalTrials.gov, Identifier: NCT02603341) that includes 1750 patients has recently begun, with the primary aim of investigating whether proton therapy reduces cardiotoxicity, compared to photon therapy, for patients with locoregional breast cancer that includes the IMNs. Hopefully, the study will show the extent to which the dose sparing seen in treatment planning studies translates into reduced risk of late effects for the patients. Until there is additional clinical evidence on long-term cardiopulmonary toxicity, the heart, LAD, and lung doses should be kept as low as possible using treatment techniques such as DI and proton therapy.

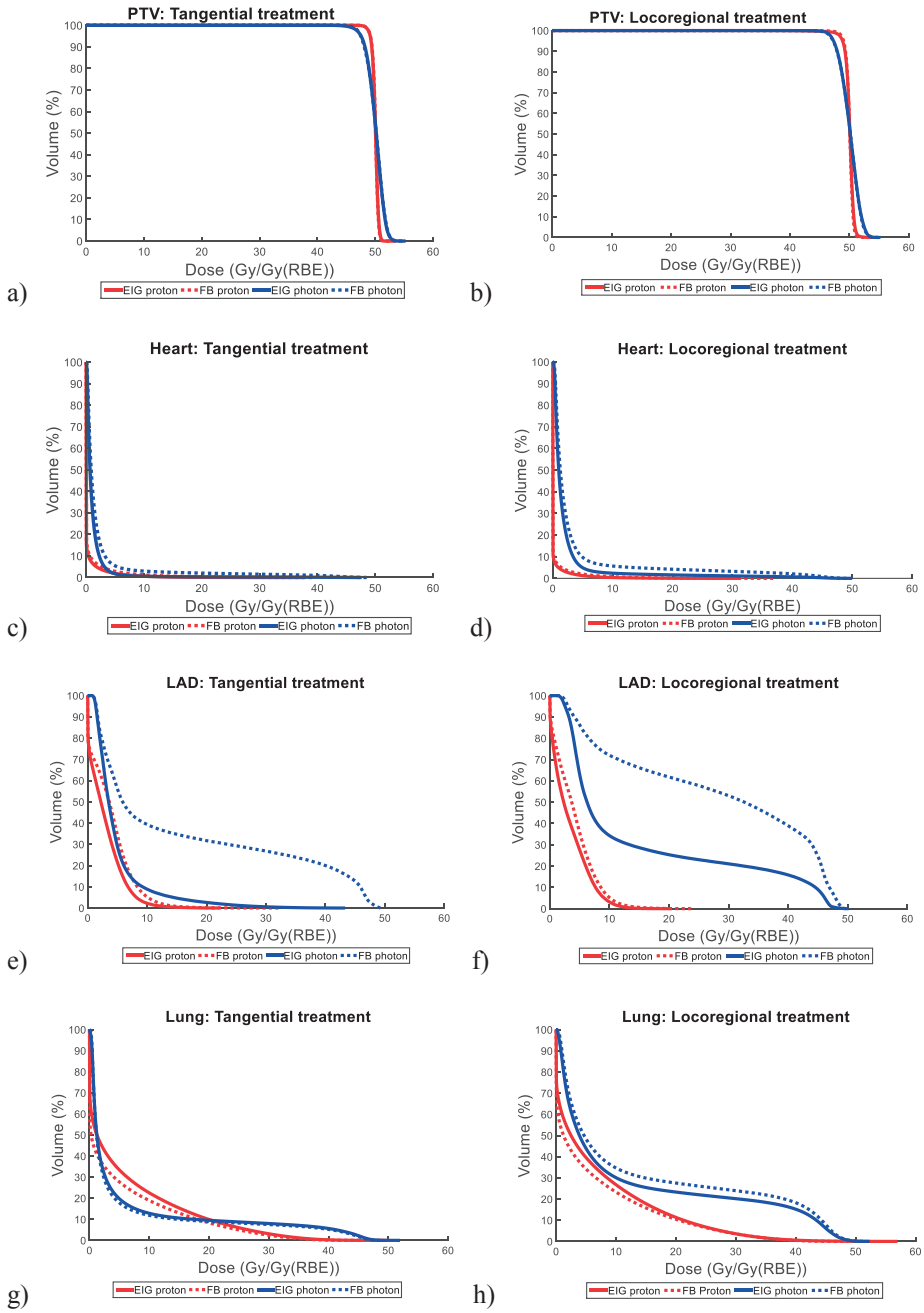

Figure 9 Average dose-volume histograms for (a,c,e,g) tangential and (b,d,f,h) locoregional treatment of left-sided breast cancer comparing enhanced inspiration gating (EIG) proton (solid red lines), free breathing (FB) proton (dashed red lines), EIG photon (solid blue lines) and FB photon (dashed blue lines) treatments for (a,b) the planning target volume (PTV), (c,d) the heart, (e,f) the left anterior descending coronary artery (LAD), and (g,h) the ipsilateral lung. All proton DVHs are for intensity modulated proton therapy.

Hodgkin's lymphoma

Hodgkin's lymphoma is cancer of the lymphoid tissue and often affects young people. In the past, it was usually treated with radiotherapy only, using large fields to cover entire nodal stations [112, 113]. Increased risk of late effects such as secondary cancer, cardiovascular disease, and pulmonary disease, have been observed [107]. Thus, the goal of radiotherapy for HL patients has been to reduce the risk of late effects while maintaining high disease control. As a result, the current treatment of HL is usually a combination of chemotherapy and involved node or involved site radiotherapy (INRT/ISRT) at a lower prescribed dose (20-30 Gy), and only the initially involved lymph nodes are irradiated, which reduces the irradiated volume [112-116]. In mediastinal HL, more conformal delivery techniques such as 3D-CRT, IMRT, VMAT, helical tomotherapy, and proton therapy [107, 113, 116-119], as well as treatment during DI [119-125], have shown the potential to deliver a reduced dose to healthy tissue. Today, delivery of both VMAT and IMPT during DI is possible [126-130]. However, information regarding the combined use of VMAT and IMPT together with DI is limited [119, 131, 132]. The study presented in **paper IV** investigated potential healthy tissue dose sparing of various combinations of delivery techniques (3D-CRT, VMAT, and IMPT) and breathing techniques (DI and FB) to find the optimal treatment technique for mediastinal HL patients. That study was the first to compare all these treatment techniques for mediastinal HL.

Patients and treatment techniques

Eighteen patients (10 female and 8 male) with mediastinal HL were included in the study of **paper IV**. Two CT images were acquired for each patient, one during DI and one during FB. For 10 patients, the DI CT image was acquired with the RPM system using EIG, and for 8 patients the image was acquired with the Sentinel system using DIBH. The median DI amplitude was 11.7 mm (range 9.0-20.7). Based on PET images acquired during FB, the CTVs were delineated in both the DI and the FB images using the ISRT technique [112]. An 8-mm isotropic CTV-to-PTV margin was added for all patients. The delineated OARs were the heart, LAD, lungs, and female breasts. Six treatment plans were created for each patient: 3D-CRT in FB, 3D-CRT in DI, VMAT in FB, VMAT in DI, IMPT in FB, and IMPT in DI. Examples of dose distributions for each treatment technique are presented in Figure 10. The treatment plans were individually optimised for each patient using the Eclipse TPS. The OAR doses were kept as low as possible. The prescribed dose was 29.75 Gy/Gy(RBE) in 17 fractions, assuming a constant RBE of 1.1 for protons. Different dosimetric parameters were retrieved from the DVHs. The HI and ID were calculated using Eqs. (1) and (2) in the same way as described for **paper II**. In

addition, the $CI_{Paddick}$ was calculated using Eq. (3). Because more than two treatment techniques were compared, Friedman tests were carried out to investigate whether the difference between any of the treatment techniques was statistically significant. If the difference was statistically significant, post-hoc two-sided paired Wilcoxon tests were then performed to determine which treatment techniques were statistically significantly different. Multiple testing was not accounted for because it was considered too conservative due to the large number of comparisons.

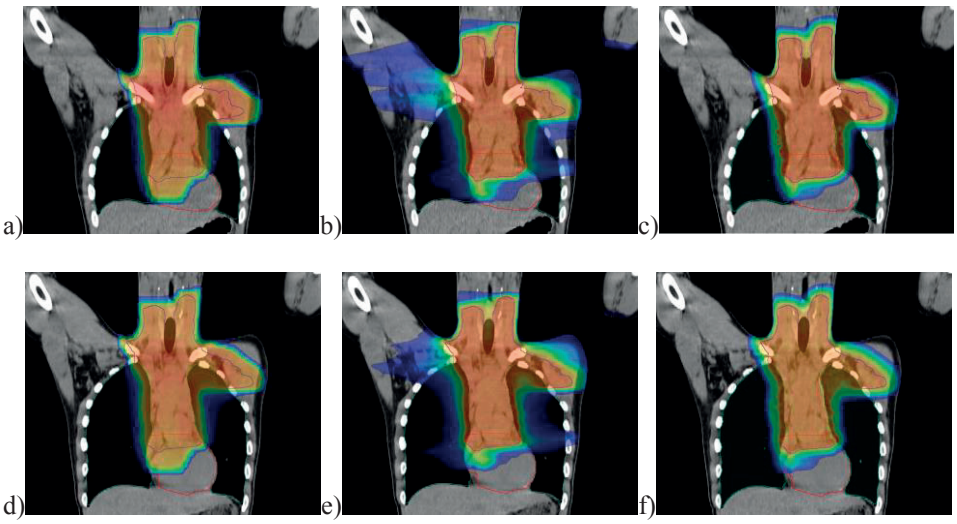

Figure 10 Coronal dose distributions (15% to maximum dose) for one mediastinal Hodgkin's lymphoma patient in **paper IV** for (a) free breathing (FB) three-dimensional conformal radiotherapy (3D-CRT), (b) FB volumetric modulated arc therapy (VMAT), (c) FB intensity modulated proton therapy (IMPT), (d) deep inspiration (DI) 3D-CRT, (e) DI VMAT, and (f) DI IMPT. The planning target volume (PTV) is outlined in blue, the heart is outlined in red, and the lungs are outlined in green.

Comparison of deep inspiration and free breathing

During DI, the lung volume increased and the mediastinum was elongated, pulling the heart caudally (Figure 10). This resulted in a smaller lung volume in the treatment fields and a larger distance between the heart and TV for most patients. As a result, the median lung D_{mean} was significantly reduced by approximately 10%-20% for DI compared to FB for all delivery techniques. For the heart, however, the benefits from using DI varied substantially among patients (Figure 11b). The median heart and LAD D_{mean} were reduced by 10%-40% and 10%-60%, respectively, when DI was used for all three delivery techniques; however, the difference reached statistical significance only for VMAT. Large heart and LAD dose reductions were observed for some patients when using DI, while the dose actually increased for other patients (Figure 11b). To find the optimal breathing technique for each patient, it is important to perform comparative treatment planning

between DI and FB. In addition, very similar target coverage was achieved for DI and FB, and there was no difference in D_{mean} to the female breasts with respect to DI and FB.

Several previous studies compared treatment during DI and FB for mediastinal HL, for both 3D-CRT and IMRT [122-125]. In accordance with **paper IV**, they all found significantly reduced lung dose using DI. However, they also found significantly reduced heart and LAD doses using DI, results observed only for VMAT in **paper IV**. Most of the previous studies did not find any significant difference in the breast dose between DI and FB [123, 125], except one that found an increase in breast dose for DI [124]. Possible reasons for the differences observed could be that smaller treatment margins were used for DI than for FB in some of the studies and the differences in disease distribution and photon treatment techniques (3D-CRT/IMRT/VMAT).

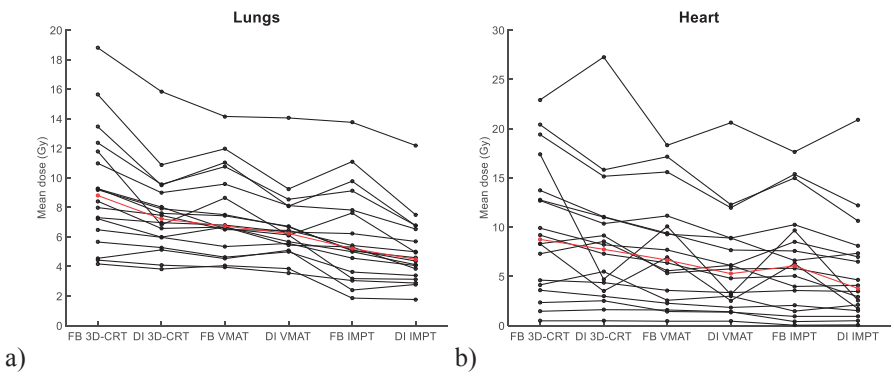

Figure 11 The individual mean dose to (a) the lungs and (b) the heart for mediastinal Hodgkin's lymphoma patients, comparing free breathing (FB) three-dimensional conformal radiotherapy (3D-CRT), deep inspiration (DI) 3D-CRT, FB volumetric modulated arc therapy (VMAT), DI VMAT, FB intensity modulated proton therapy (IMPT), and DI IMPT. The values for each patient are shown in black and the median values for the whole patient cohort in red. Adopted from **paper IV**.

Comparison of IMPT, VMAT, and 3D-CRT

Both IMPT and VMAT improved the target coverage and resulted in more conformal dose distributions compared to 3D-CRT, which generally decreased the OAR doses (Figure 10, Figure 11 and Figure 12). The use of IMPT was more beneficial than VMAT because it reduced the OAR doses for all dose levels, while VMAT reduced the volumes that received high doses, but at the expense of increasing the low-dose volumes (Figure 10 and Figure 12). The median lung, heart, and breast D_{mean} were significantly reduced by approximately 20%-40%, 10%-50% and 60%-90%, respectively, for IMPT compared to VMAT and 3D-CRT. In addition, the ID was reduced by approximately 50% for IMPT compared to VMAT

and 3D-CRT. This reduction in the ID could reduce the risk of secondary cancer [107]. These results are in agreement with those found in previous studies that compared proton and photon treatments during FB [107].

In general, the lowest OAR doses were observed for the combination of IMPT and DI (Figure 11 and Figure 12). This agreed with the results observed by Rechner et al. [131], which was the only study preceding **paper IV** that compared proton and photon therapy during both DI and FB for mediastinal HL. However, in other respects, the results obtained in **paper IV** differed from those in Rechner et al. In general, the results in **paper IV** showed greater healthy tissue sparing with proton therapy compared to photon therapy, whereas the results in Rechner et al. showed greater benefit with DI compared to FB. The study by Baues et al. [132] was the only study preceding **paper IV** that compared IMPT and VMAT during DI for mediastinal HL. It showed reductions in OAR D_{mean} using IMPT, comparable to the reductions presented in **paper IV**. However, in contrast to **paper IV**, the Baues et al. study also showed a decrease in the lung V_{20Gy} for IMPT compared to VMAT. The results of **paper IV** have contributed to the clinical implementation of DI photon therapy for mediastinal HL at Skåne University Hospital in 2014 and DI proton therapy at the Swedish proton center, the Skandion clinic, in Uppsala in 2018.

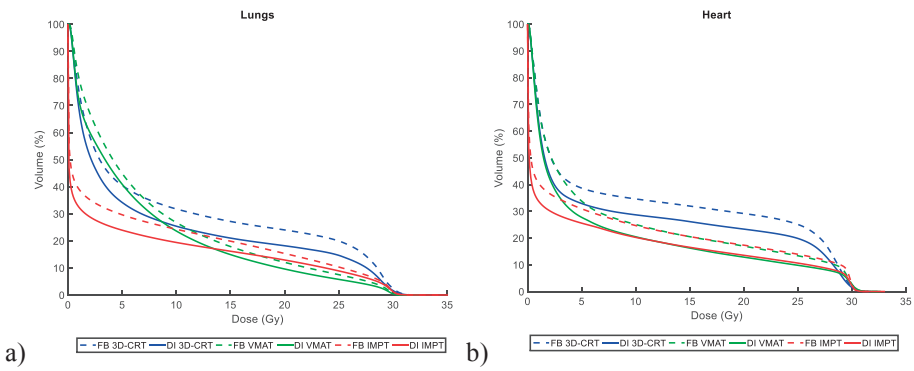

Figure 12 Average dose-volume histograms for mediastinal Hodgkin's lymphoma comparing deep inspiration (DI) (solid lines) with free breathing (FB) (dashed lines) in intensity modulated proton therapy (IMPT) (red), volumetric modulated arc therapy (VMAT) (green) and three-dimensional conformal radiotherapy (3D-CRT) (blue), for (a) the lungs and (b) the heart. Adopted from **paper IV**.

Dosimetric effects of breathing motion

A limitation of **paper IV** is that it was a pure treatment planning study and the effects of intrafractional breathing motion were not considered. The inclusion of these effects could result in a degradation of the dose distribution to the TV and OARs due to dose blurring, interplay effects, and range uncertainties [2, 29, 36, 37]. This degradation would probably affect the comparison of the different delivery

techniques, because breathing motion has the largest impact on IMPT plans and the smallest impact on 3D-CRT plans. However, if repainting or a large spot size is used, the impact of interplay effects on PBS plans during FB for mediastinal HL has been shown to be small [133]. Also, robust optimisation could be used to account for the effects of breathing motion [134, 135].

Treatment during DI could also reduce intrafractional breathing motion, and thus reduce the treatment margins needed. This aspect was not included in **paper IV**, where the observed healthy tissue dose sparing was achieved through anatomical changes only. However, treatment is delivered during several breath-holds, raising concerns about the impact of inter-breath-hold variations, which was investigated for photon therapy of breast cancer in **paper III**. These variations may pose a greater problem for treatment of mediastinal HL because the TV is not as superficially located as the breast. Hence, a poorer correlation between the TV and external marker movements may be expected. In addition, the dosimetric impact of inter-breath-hold variations would be greater for proton therapy than for photon therapy. Enmark et al. [136] showed that there was noticeable dosimetric impact of anatomical inter-breath-hold variations for proton PBS treatment of mediastinal HL for a single fraction, but the effects were averaged out for an entire treatment. Data on the dosimetric effects of breathing motion during both FB and DI, for mediastinal HL, are limited, and more studies, especially for proton PBS, would be desirable.

Interplay effects for VMAT radiotherapy

In many cases, the use of VMAT for tumours in the thorax and abdomen would be preferable because it produces more conformal dose distributions than 3D-CRT [17]. However, breathing motion is a concern and interplay effects have been shown for individual treatment fractions [2-8, 137-147]. The extent of interplay effects depends on different patient- and machine-specific parameters, such as the breathing pattern [6, 137, 140-142, 147], dose level [7, 147], dose rate [4, 8, 137, 140, 147], collimator angle [137, 147], and the complexity of the treatment plan [6, 8, 141, 145-147]. However, the dosimetric effects of interplay have been shown to average out for multiple fractions [2-8, 147]. Therefore, the impact of interplay effects probably is greatest for SBRT, in which few fractions are delivered [7, 140-146]. Although the total dose distribution is homogeneous, an unpredictable heterogeneous dose distribution is delivered for each fraction. This results in different parts of the tumour being underdosed from fraction to fraction, the biological consequences of which are still not well known. Several different approaches have been used to investigate interplay effects, including statistical analysis [3], simulations [7, 137, 138, 142-145, 147], and measurements [4-6, 8, 137, 139-141]. Simulations are advantageous compared to measurements because they are relatively fast and thereby allow a large number of treatment scenarios to be investigated. In **paper V**, a tool to simulate interplay effects for VMAT using a commercial TPS was developed and verified with dosimetric measurements. The simulation tool was then used to conduct a large systematic investigation of how the extent of interplay effects varies with different patient- and machine-specific parameters. In **paper VI**, the simulation tool was further adjusted for use in a more clinical setting, to estimate the dosimetric impact of interplay effects for actual patient treatments.

Simulations of interplay effects

For the simulations and measurements performed in **paper V**, several VMAT plans were created using the Eclipse TPS on a virtual phantom of the Delta4 (Scandidos, Uppsala, Sweden) (Figure 13). The virtual phantom contained spherical CTVs of various sizes and two cylindrical OARs. To account for the maximum motion extent, ITVs corresponding to the simulated breathing amplitudes were created and a 5-mm isotropic PTV margin was added.

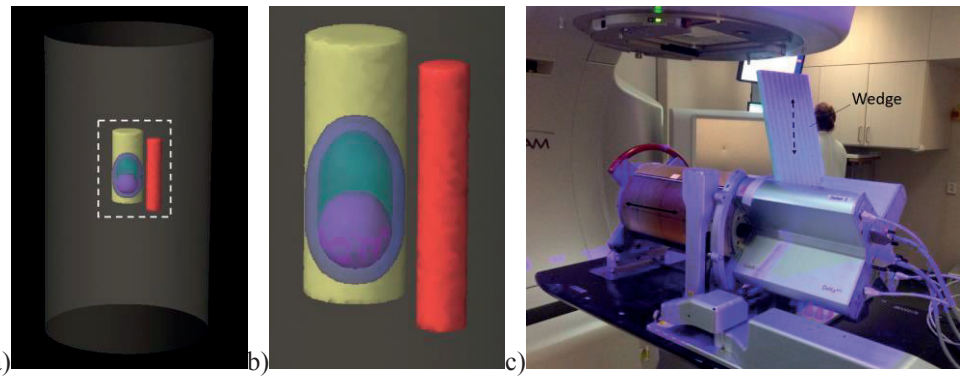

Figure 13 (a) Virtual phantom of the Delta4 used for simulations of interplay effects, containing a clinical target volume (purple), internal target volume (green), planning target volume (blue) and two organs at risk (yellow and red). (b) Enlarged view of the white dashed box in (a). (c) Real Delta4 phantom, positioned on the HexaMotion platform in the setup used for the verification measurements. Adopted from **paper V**.

Simulation tool

Using an in-house developed program [148, 149], the original treatment plan was divided into several smaller sub-arcs, where each sub-arc corresponded to the treatment delivered during a short time interval. The isocenter of each sub-arc was then shifted to simulate breathing motion. The $\sin^6$ breathing pattern in the CC direction, chosen for the simulations (Figure 14a), had varying amplitudes, respiratory period times, and initial breathing phases to mimic real patient breathing [34, 150]. Rigid motion was simulated by shifting the isocenter relative to the entire phantom, resulting in a treatment plan containing several hundred sub-arcs, with the isocenter of each sub-arc being shifted (Figure 14b). The treatment plan was calculated in the TPS, and a simulated dose distribution, which included the effects of breathing motion, both dose blurring and interplay effects, was generated. Convolving the original static dose distribution with the motion function yielded a dose distribution that included only dose blurring [2, 139]. This convolved dose distribution was then subtracted from the simulated dose distribution, so the residual dose differences could be interpreted as solely due to interplay effects. The relative

dose differences to 98% and 2% of the CTV ($\Delta D_{98\%}$ and $\Delta D_{2\%}$) were calculated, which correspond to the near minimum- and maximum dose differences.

The developed simulation tool allows the different effects of motion to be separated so the effect of interplay can be studied separately. The tool is also relatively fast, allowing many different treatment scenarios to be investigated. However, dose calculation is time consuming due to the large number of generated sub-arcs. By optimising the number of sub-arcs, the calculation time could be reduced, which would allow even more treatment scenarios to be investigated. Another limitation of the simulation tool is that it is based on a $\sin^6$ motion pattern, which implies perfect cyclic respiration. However, cyclic breathing does not represent real patient breathing, which tends to be irregular, with a variable amplitude and period time as well as baseline drifts [34, 35]. In addition, the simulation tool includes only rigid motion, and deformations and changes in the radiological pathlength are not accounted for. The simulation tool is valid only for VMAT plans optimised using the Eclipse TPS. The extent of interplay effects may be different for plans from other TPSs because their optimisers work differently and, for example, other MLC sequences are generated.

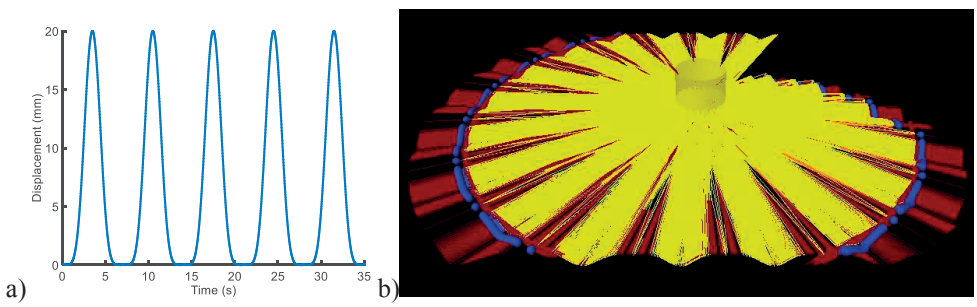

Figure 14 (a) $\sin^6$ breathing pattern with an amplitude of 20 mm and a period time of 7 s. (b) Volumetric modulated arc therapy (VMAT) plan divided into sub-arcs, where the isocenter of each sub-arc has been shifted according to the breathing pattern in (a). Adopted from **paper V**.

Verification measurements

To verify the simulation tool, dose distributions from measurements were compared to correspondingly simulated dose distributions. Five different treatment plans were delivered to the Delta4 phantom positioned on the motion platform HexaMotion (Scandidos) (Figure 13c), which was either static or moving during irradiation. The OS system was used to synchronise the treatment delivery with the phantom motion. The same treatment plans and motion patterns were used for both the simulations and the measurements. The results showed good agreement between the measured and the simulated dose distributions during motion, and were comparable to the agreement of the results obtained for the measured and simulated static dose

distributions. On the basis of these results, the simulation tool was considered validated and could be used for further simulations.

Patient- and machine-specific parameters

The developed simulation tool was then used to study how the extent of interplay effects depends on different patient- and machine-specific parameters. The patient-specific parameters investigated were the CTV size and the breathing pattern. Seventy-two breathing patterns were created by combining six different breathing amplitudes, three period times, and four initial breathing phases. The machine-specific parameters investigated were the use of flattening-filtered (FF) or FFF treatment (dose rate), dose level, collimator angle, and plan complexity. Seventeen different VMAT plans were created by varying these parameters. Different plan complexities were achieved by varying the number of monitor units (MU)/Gy. A plan with a high MU/Gy has more MLC movement and smaller field openings and could therefore be more susceptible to interplay effects. A total of 136 simulations were performed for one treatment fraction using different combinations of VMAT plans, CTV sizes, and breathing patterns. To investigate interplay effects for multiple fractions, the average dose distribution for the four different initial breathing phases was calculated and compared to the convolved dose distribution.

Considerable interplay effects were observed within the CTV for single fractions and their extent depended largely on the different patient- and machine-specific parameters simulated (Figure 15). Both under- and overdosed volumes were observed, with minimum $\Delta D_{98\%}$ and maximum $\Delta D_{2\%}$ of -16.7% and 16.2%, respectively, and values in the range of 10%-15% were common. The extent of interplay effects was larger for FFF than for FF and generally increased with higher breathing amplitudes, longer period times, lower dose levels, and more complex treatment plans (Figure 15). These dependencies all agreed with those found in previous studies [4, 6-8, 137, 140-142, 145, 146]. However, no single study has investigated the dependence of interplay effects on all these parameters for VMAT before. The increase in interplay effects observed with longer period times, lower dose levels, and FFF (higher dose rate) is due to less intrafraction averaging, i.e., interplay effects average out to a lesser extent when fewer respiratory cycles pass while the plan is delivered. Although trends in the dependence of interplay effects on the different parameters were observed, large fluctuations were present (Figure 15). In addition, the interplay effects varied considerably with the initial breathing phase, and larger variations in $\Delta D_{98\%}$ and $\Delta D_{2\%}$ were observed for smaller CTVs. These variations were due to interference from particular combinations of breathing patterns and machine-specific parameters, which make interplay effects for real patient treatments extremely difficult to predict. Only small differences in $\Delta D_{98\%}$ and $\Delta D_{2\%}$ were observed for different collimator angles, in contrast with the results

found by Court et al. [137], which showed larger interplay effects for parallel motion between the MLCs and the TV for IMRT than for perpendicular motion. When multiple fractions were simulated, the extent of the interplay effects decreased (Figure 15) because of interfraction averaging, which was in agreement with previous studies [2-8]. However, whether this averaging also applies to the biological effect is not known. Thus, investigating interplay effects for individual fractions and not just for the total accumulated dose of the whole treatment could be important. The interplay effects could be mitigated by wise selection of the machine-specific parameters, for example, reduce the complexity of the treatment plan, reduce the dose rate (i.e., use FF instead of FFF), or reduce both. However, reducing the dose rate leads to prolonged treatment times, thus increasing the likelihood of patient motion during treatment delivery. In addition, care should be taken before using VMAT for patients with large tumour motion and long period times.

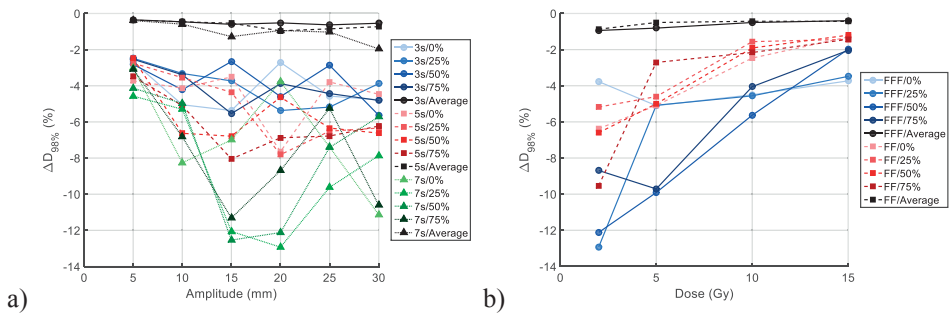

Figure 15 Depencence of interplay effects on (a) the breathing amplitude and period time, and (b) the dose level for flattening-filtered (FF) and flattening-filter free (FFF) treatment, presented as the relative dose differences to 98% of the clinical target volume ($\Delta D_{98\%}$). The different initial breathing phases are displayed in different colour shades and the effect of multiple fractions is displayed in black. The lines are for illustration only. The corresponding figures for all parameters investigated are presented in **paper V**.

Clinical application

To estimate interplay effects for real patient treatments, including those caused by anatomical deformations from breathing, the simulation tool in **paper VI** was modified for application to patient 4DCT images and DIR was used to dynamically accumulate the dose. This modified simulation method was then used to investigate interplay effects for FFF VMAT SBRT for liver tumours, which have been investigated in only a few studies [144-146, 151]. None of these studies investigated FFF treatment, and anatomical deformations were considered for only a few patients by Kuo et al. [146]. Large interplay effects would be expected with FFF VMAT SBRT for liver tumours because of large tumour motion [35, 151-153], low

interfraction averaging (few fractions) [144-146, 151], and low intrafraction averaging (short delivery times) [21]. In addition, one can assume the treatment plans to be quite complex because the tumour is adjacent to many radiation-sensitive OARs, such as the liver and bowel [145]. As shown in **paper V**, the combination of high-complexity FFF VMAT plans and large tumour motion may be very susceptible to interplay effects.

Free breathing 4DCT images for 10 liver SBRT patients, which represented a large range of tumour motions and GTV sizes, were included in **paper VI**. The 4DCT images were acquired using the Anzai pressure belt without abdominal compression. To simulate clinically relevant treatment conditions, the delineation of TVs and OARs and the generation of treatment plans were based on the NRG-BR001 protocol (ClinicalTrials.gov, Identifier: NCT02206334). NRG-BR001 is a phase I study of SBRT for treating oligometastatic prostate, breast, and lung cancers to establish the safety and efficacy of SBRT in treating multiple metastases (including metastases in the liver) within a single treatment course. Based on the GTV, an ITV was created in the mid-ventilation phase, with individual margins based on the maximum motion relative to the mid-ventilation phase in the CC, AP, and LR directions. A PTV was then generated by adding 5-mm margins in the LR and AP directions and a 7-mm margin in the CC direction. 10 MV FFF VMAT plans (maximum dose rate = 2400 MU/min), with the prescribed dose of 45 Gy in three fractions, were created using the Eclipse TPS.

To generate dose distributions that include the effects of motion, i.e., both interplay effects and dose blurring, each plan was divided into phase-specific sub-plans using the simulation tool developed in **paper V** that were calculated on the corresponding phase of the 4DCT image (Figure 5). A blurred dose distribution that did not include interplay effects was also obtained by distributing the delivery of the whole plan uniformly over all phases. The total dose distributions were accumulated at the mid-ventilation phase using the DVFs from DIR between the corresponding CT and the mid-ventilation phase CT. Hence, three different dose distributions were generated for each patient (Figure 16):

- *Original static dose distribution:* Original dose distribution at the mid-ventilation phase that does not include any effects of motion
- *Dose distribution without interplay:* Simulated dose distribution that includes the effects of dose blurring but not interplay effects
- *Dose distribution with interplay:* Simulated dose distribution that includes both dose blurring and interplay effects

For each dose distribution, $D_{98\%}$, $D_{2\%}$, D_{mean}, and HI [Eq. (1)] within the GTV were calculated. In addition, $\Delta D_{98\%}$ and $\Delta D_{2\%}$ were calculated for the difference between the dose distributions with and without interplay. By comparing these dose

distributions, it was possible to separate the interplay effects from dose blurring. All simulations were performed for a single fraction. Friedman tests were carried out to determine if the difference between the three dose distributions was significant. If a significant difference was observed, post-hoc two-sided paired Wilcoxon tests were carried out and multiple testing was accounted for with a Bonferroni correction.

The dose distribution without interplay effects was more homogeneous than the original static dose distribution because the heterogeneities within the GTV in the original plan were blurred (Figure 16b). The dose distributions were more heterogeneous when interplay effects were included (Figure 16c). Comparison of the dose distributions with and without interplay effects included showed that $D_{98\%}$ decreased for 9 of the 10 patients and $D_{2\%}$ increased for all patients, resulting in a higher HI for all patients. The median $\Delta D_{98\%}$ and $\Delta D_{2\%}$ were -4.0% (range -7.0% to -1.5%) and 4.1% (range 2.5% to 4.9%), respectively. When the total effect of motion was considered (by comparing the dose distribution with interplay and the original static dose distribution), the differences in the dosimetric parameters were slightly smaller because the interplay effects were partly cancelled out by the dose blurring. However, significant differences in $D_{98\%}$, $D_{2\%}$, and HI were still observed.

The interplay effects observed in **paper VI** were larger than those in previous studies, for both liver and lung SBRT [7, 140-146, 151], probably because a high dose rate (2400 MU/min) in combination with a relatively long period time (5 s) was simulated for a single fraction, thus minimising both the intrafractional and the interfractional averaging. These simulation conditions were chosen because they were considered clinically relevant worst-case scenarios and generated large interplay effects in **paper V**. The simulation method developed in **paper VI** has the advantage of accounting for breathing-induced deformations because it is based on 4DCT images and DIR. **Paper VI** was the first study that investigated breathing-induced interplay effects for FFF VMAT SBRT for liver tumours, including deformations. However, it was limited to the motion that occurred during the 4DCT scan, which may not be representative of the motion that occurs during treatment delivery [151, 152, 154]. Another limitation of **paper VI** is that simulations were performed for only one initial breathing phase for a single treatment fraction, although in **paper V** both the initial breathing phase and the fractionation had a large impact on the extent of interplay effects. In addition, uncertainties in the DIR may have affected the accuracy of the dose accumulation.

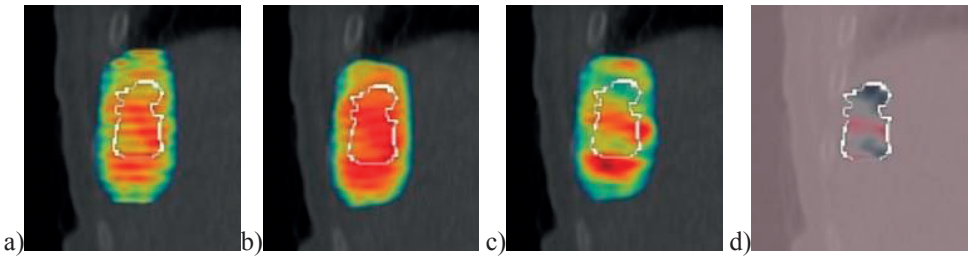

Figure 16 Examples of (a) an original static dose distribution, (b) a dose distribution with dose blurring, and (c) a dose distribution with both dose blurring and interplay effects, for stereotactic liver volumetric modulated arc therapy. (d) The difference between the dose distributions in (b) and (c), with negative and positive dose differences indicated in blue and red, respectively. The white lines correspond to the gross tumour volume (GTV). Adopted from **paper VI**.

Conclusions

In this thesis, major dosimetric effects of breathing motion on radiotherapy treatment were demonstrated. Knowledge of these effects is important for the ability to individually optimise the radiotherapy treatment. Beneficial effects were observed when the patient used controlled deep inspiration (DI). It reduced the dose to the organs at risk (OARs) while maintaining the dose to the target. Photon treatment of left-sided breast cancer during DI reduced the doses to the heart, left anterior descending coronary artery, and lung (**papers I and III**). Based on normal tissue complication probability calculations, these dose reductions could translate into reduced risk of late effects (**paper I**). Good intrafractional deep inspiration breath-hold (DIBH) reproducibility was observed; hence, reduced OAR doses were maintained during treatment delivery to the patient (**paper III**). However, large intrafractional DIBH variations were observed for a few treatment fractions. This could affect the target coverage and OAR doses negatively, so a good motion-monitoring strategy is important. Proton therapy during both DI and free breathing (FB) generally reduced OAR doses beyond what could be achieved with DI photon therapy (**paper II**). For mediastinal Hodgkin's lymphoma (HL), the use of DI and proton therapy generally reduced OAR doses compared to FB and photon therapy (**paper IV**). However, because multiple OARs are considered and there is a large variation in disease distribution, there is not a single best treatment technique for all mediastinal HL patients, and both the breathing- and delivery techniques should be chosen individually for each patient.

Breathing-motion-induced interplay effects were shown to negatively affect the dose distribution for volumetric modulated arc therapy (VMAT), resulting in the underdosing of part of the tumour. The extent of interplay effects depended on the tumour motion and treatment plan characteristics (**paper V**). The interplay effects generally increased for higher breathing amplitudes, longer period times, lower dose levels, higher dose rates (flattening-filter free), and more complex treatment plans. Selecting these treatment delivery parameters wisely can mitigate the interplay effects. Furthermore, investigation of interplay effects in real patient treatments of liver metastases using flattening-filter free stereotactic VMAT showed that parts of the tumour could be underdosed up to 7% (**paper VI**).

Future perspectives

There are clear dosimetric benefits of using DI treatment for left-sided breast cancer, but the benefits are less clear for mediastinal HL due to the large differences in disease distribution from patient to patient. More studies are needed to determine which HL patients would benefit from DI treatment. In addition, further investigation of the dosimetric consequences of both intrafractional breathing motion and DIBH variability is warranted, especially for IMPT. Treatment during DI could also be beneficial for other diagnoses such as lung and liver tumours, but such treatment is more complex because the tumour motion is less correlated with the movement of the chest wall, and further research is required.

To better understand the complexity of breathing-induced interplay effects in the treatment of moving tumours, further investigations that includes more treatment scenarios and diagnoses are needed. The simulation tool developed in **papers V and VI** could be further developed for use with IMPT, for which the interplay effects are larger than those for VMAT. Interplay effects also could result in undesired hotspots within the OARs, which needs to be further investigated. Ideally, the simulations performed should be for realistic treatment conditions, including breathing-induced anatomical deformations and tumour motion representative of an entire treatment delivery. Four-dimensional magnetic resonance imaging (4D MRI), which allows for time-resolved volumetric imaging during a time span representative of treatment delivery, could be used to achieve realistic simulations. Four-dimensional MRI could also be used to acquire images during multiple DIBHs, thus allowing further investigation of the dosimetric effects of inter-breath-hold variations. Altogether, such simulation method would enable investigation of the delivered dose to the patient, including various uncertainties, instead of only the planned dose. Ultimately, this information could be used to provide clinical guidelines about when it is safe to treat moving tumours using different treatment techniques.

This thesis has shown that breathing motion may have both positive and negative effects on the dose distribution in radiotherapy. However, the clinical impact of these dosimetric effects for the patient remains to be investigated. To date, no study has shown that the use of DI and protons actually reduces late effects in current breast cancer and HL radiotherapy. In addition, further research is needed to determine the clinical impact of the dose heterogeneities caused by interplay effects.

The interplay effects average out dosimetrically when multiple fractions are delivered; however, the biological effect of the dose heterogeneities delivered at each fraction is not fully known. The biological effect could be further investigated with *in vivo* studies on mice using a small-animal radiotherapy system that can deliver dose distributions that include hot and cold spots corresponding to interplay effects.

Acknowledgements

En avhandling är inget man producerar själv och jag är helt övertygad om att denna avhandling aldrig hade blivit skriven om det inte varit det stöd jag på olika sätt fått från en rad olika människor. Jag skulle speciellt vilja tacka

Min huvudhandledare *Sofie Ceberg*, för att du fick mig intresserad av forskning. Tack för att du alltid ställer upp, ditt brinnande engagemang och din positiva inställning. Du inspirerar mig och är en fantastisk förebild. Utan ditt stöd hade jag aldrig vågat. Och tack för alla roliga resor och för den fina traditionen att fira varje ny publikation med bubbel!

Min biträdande handledare *Crister Ceberg,* för din enorma kunskap, ditt engagemang och för att du alltid tar dig tid att hjälpa till. Tack för alla intressanta diskussioner och för att du alltid utmanat mig att tänka utanför min comfort zone!

Min biträdande handledare *Sven Bäck*, för dina kloka råd och de möjligheter du gett mig, både till forskning och kliniskt arbete. Tack för att du alltid har trott på mig, även när jag inte har trott på mig själv!

Alla mina vänner och kollegor på avdelningen för medicinsk strålningsfysik, Lunds universitet, och strålbehandlingen, Skånes universitetssjukhus, som på olika sätt hjälpt och stöttat mig!

Alla mina medförfattare för ert stöd och er uppmuntran. Utan er hade det inte funnits några artiklar att basera denna avhandling på. Ett speciellt tack till *Malin Kügele* och *Fredrik Nordström* för ovärderligt samarbete!

Anna Stenvall, för att jag haft den stora förmånen att få dela kontor med dig under dessa år. Tack för att du stått ut med röran på mitt skrivbord och för att jag fått ”kräka av mig” med jämna mellanrum!

Mina kursare på sjukhusfysikerprogrammet vid Lunds universitet för er vänskap och ovärderliga uppmuntran under studietiden. Utan er hade jag aldrig blivit sjukhusfysiker!

Min familj och mina vänner, som på olika sätt stöttat mig. Tack för att ni alltid lyckas få mig på gott humör!

Min bror *Jonas*, *Sara* och *Ofelia* för alla roliga stunder!

Mamma och pappa, för att ni alltid har stöttat mig och ställt upp, oavsett vad det har gällt. För den trygghet ni har givit mig och för att jag alltid har haft möjligheten att ”komma hem”. Nu blev det en doktorsavhandling, men jag vet att ni varit lika stolta oavsett vad jag hade gjort i livet!

Min underbara sambo *Patrik,* för att du stått ut med mig under skrivandet av denna avhandling. Att komma hem till dig efter en lång arbetsdag är det bästa jag vet. Du gör mig oerhört lycklig! Älskar dig mer än mest!

References

1. Keall PJ, Mageras GS, Balter JM, Emery RS, Forster KM, Jiang SB, et al. The management of respiratory motion in radiation oncology report of AAPM Task Group 76. Med Phys. 2006;33(10):3874-900.
2. Bortfeld T, Jiang SB, Rietzel E. Effects of motion on the total dose distribution. Semin Radiat Oncol. 2004;14(1):41-51.
3. Bortfeld T, Jokivarsi K, Goitein M, Kung J, Jiang SB. Effects of intra-fraction motion on IMRT dose delivery: statistical analysis and simulation. Phys Med Biol. 2002;47:2203-20.
4. Jiang SB, Pope C, Al Jarrah KM, Kung JH, Bortfeld T, Chen GT. An experimental investigation on intra-fractional organ motion effects in lung IMRT treatments. Phys Med Biol. 2003;48:1773-84.
5. Duan J, Shen S, Fiveash JB, Popple RA, Brezovich IA. Dosimetric and radiobiological impact of dose fractionation on respiratory motion induced IMRT delivery errors: a volumetric dose measurement study. Med Phys. 2006;33(5):1380-7.
6. Court L, Wagar M, Berbeco R, Reisner A, Winey B, Schofield D, et al. Evaluation of the interplay effect when using RapidArc to treat targets moving in the craniocaudal or right-left direction. Med Phys. 2010;37(1):4-11.
7. Rao M, Wu J, Cao D, Wong T, Mehta V, Shepard D, et al. Dosimetric impact of breathing motion in lung stereotactic body radiotherapy treatment using intensity modulated radiotherapy and volumetric modulated arc therapy. Int J Radiat Oncol Biol Phys. 2012;83(2):251-6.
8. Netherton T, Li Y, Nitsch P, Shaitelman S, Balter P, Gao S, et al. Interplay effect on a 6-MV flattening-filter-free linear accelerator with high dose rate and fast multi-leaf collimator motion treating breast and lung phantoms. Med Phys. 2018;45(6):2369-76.
9. Boda-Heggemann J, Knopf AC, Simeonova-Chergou A, Wertz H, Stieler F, Jahnke A, et al. Deep Inspiration Breath Hold-Based Radiation Therapy: A Clinical Review. Int J Radiat Oncol Biol Phys. 2016;94(3):478-92.
10. Korreman SS. Motion in radiotherapy: photon therapy. Phys Med Biol. 2012;57(23):161-91.
11. ICRU Report 83. Prescribing, Recording, and Reporting Intensity-Modulated Photon-Beam Therapy (IMRT). 2010.
12. ICRU Resport 50. Prescribing, Recording, and Reporting Photon Beam Therapy. 1993.
13. ICRU Report 62. Prescribing, Recording, and Reporting Photon Beam Therapy (Supplement to ICRU Report 50). 1999.

14. Particle Therapy Co-Operative Group (PTCOG), http://www.ptcog.ch/index.php/facilities-in-operation [2018-08-17].
15. Intensity Modulated Radiation Therapy Collaborative Working Group. Intensity-modulated radiotherapy: current status and issues of interest. Int J Radiat Oncol Biol Phys. 2001;51:880-914.
16. Otto K. Volumetric modulated arc therapy: IMRT in a single gantry arc. Med Phys. 2008;35(1):310-7.
17. Teoh M, Clark CH, Wood K, Whitaker S, Nisbet A. Volumetric modulated arc therapy: a review of current literature and clinical use in practice. Br J Radiol. 2011;84:967-96.
18. Lax I, Blomgren H, Naslund I, Svanstrom R. Stereotactic radiotherapy of malignancies in the abdomen. Methological aspects. Acta Oncol. 1994;33(6):677-83.
19. Goodman KA, Kavanagh BD. Stereotactic Body Radiotherapy for Liver Metastases. Semin Radiat Oncol. 2017;27(3):240-6.
20. Georg D, Knoos T, McClean B. Current status and future perspective of flattening filter free photon beams. Med Phys. 2011;38(3):1280-93.
21. Reggiori G, Mancosu P, Castiglioni S, Alongi F, Pellegrini C, Lobefalo F, et al. Can volumetric modulated arc therapy with flattening filter free beams play a role in stereotactic body radiotherapy for liver lesions? A volume-based analysis. Med Phys. 2012;39(2):1112-8.
22. Bignardi M, Cozzi L, Fogliata A, Lattuada P, Mancosu P, Navarria P, et al. Critical appraisal of volumetric modulated arc therapy in stereotactic body radiation therapy for metastases to abdominal lymph nodes. Int J Radiat Oncol Biol Phys. 2009;75(5):1570-7.
23. Newhauser WD, Zhang R. The physics of proton therapy. Phys Med Biol. 2015;60(8):155-209.
24. Koehler AM, Schneider JR, Sisterson JM. Flattening of proton dose distributions for large-field radiotherapy. Med Phys. 1977;4:297-301.
25. Koehler AM, Schneider JR, Sisterson JM. Range modulators for protons and heavy ions. Nucl Instrum Methods. 1975;131:437-40.
26. Kanai T, Kanai K, Kumamoto Y, Ogawa H, Yamada T, Matsuzawa H. Spot scanning system for proton radiotherapy. Med Phys. 1980;7:365-7.
27. Pedroni E, Bacher R, Blattmann H, Boehringer T, Coray A, Lomax AJ, et al. The 200 MeV proton therapy project at PSI: conceptual design and practical realization. Med Phys. 1995;22:37-53.
28. Lomax AJ, Boehringer T, Coray A, Egger E, Goitein G, Grossmann M, et al. Intensity modulated proton therapy: a clinical example. Med Phys. 2001;28(3):317-24.
29. Lomax AJ. Intensity modulated proton therapy and its sensitivity to treatment uncertainties 2: the potential effects of inter-fraction and inter-field motions. Phys Med Biol. 2008;53(4):1043-56.
30. ICRU report 78. Prescribing, recording, and reporting proton-beam therapy. 2007.

31. Paganetti H. Relative biological effectiveness (RBE) values for proton beam therapy. Variations as a function of biological endpoint, dose, and linear energy transfer. Phys Med Biol. 2014;59:419-72.
32. Goitein M. Organ and tumor motion: an overview. Semin Radiat Oncol. 2004;14(1):2-9.
33. Dawson LA, Jaffray DA. Advances in image-guided radiation therapy. J Clin Oncol. 2007;25(8):938-46.
34. Seppenwoolde Y, Shirato H, Kitamura K, Shimizu S, Van Herk MB, Lebesque JV, et al. Precise and real-time measurements of 3D tumor motion in lung due to breathing and heartbeat, measured during radiotherapy. Int J Radiat Oncol Biol Phys. 2002;53(4):822-34.
35. Shirato H, Seppenwoolde Y, Kitamura K, Onimura R, Shimizu S. Intrafractional tumor motion: lung and liver. Semin Radiat Oncol. 2004;14(1):10-8.
36. Bert C, Durante M. Motion in radiotherapy: particle therapy. Phys Med Biol. 2011;56(16):113-44.
37. Phillips MH, Pedroni E, Blattmann H, Boehringer T, Coray A, Scheib S. Effects of respiratory motion on dose uniformity with a charged particle scanning method. Phys Med Biol. 1992;37(1):223-34.
38. Damkjaer SM, Aznar MC, Pedersen AN, Vogelius IR, Bangsgaard JP, Josipovic M. Reduced lung dose and improved inspiration level reproducibility in visually guided DIBH compared to audio coached EIG radiotherapy for breast cancer patients. Acta Oncol. 2013;52(7):1458-63.
39. Knopf AC, Hong TS, Lomax A. Scanned proton radiotherapy for mobile targets-the effectiveness of re-scanning in the context of different treatment planning approaches and for different motion characteristics. Phys Med Biol. 2011;56(22):7257-71.
40. Ford EC, Mageras GS, Yorke E, Ling CC. Respiration-correlated spiral CT: A method of measuring respiratory-induced anatomic motion for radiation treatment planning. Med Phys. 2003;30(1):88-97.
41. Vedam SS, Keall PJ, Kini VR, Mostafavi H, Shukla HP, Mohan R. Acquiring a four-dimensional computed tomography dataset using an external respiratory signal. Phys Med Biol. 2003;48:45-62.
42. Underberg RW, Lagerwaard FJ, Slotman BJ, Cuijpers JP, Senan S. Use of maximum intensity projections (MIP) for target volume generation in 4DCT scans for lung cancer. Int J Radiat Oncol Biol Phys. 2005;63(1):253-60.
43. Wolthaus JW, Sonke JJ, van Herk M, Damen EM. Reconstruction of a time-averaged midposition CT scan for radiotherapy planning of lung cancer patients using deformable registration. Med Phys. 2008;35(9):3998-4011.
44. Wolthaus JW, Schneider C, Sonke JJ, van Herk M, Belderbos JS, Rossi MM, et al. Mid-ventilation CT scan construction from four-dimensional respiration-correlated CT scans for radiotherapy planning of lung cancer patients. Int J Radiat Oncol Biol Phys. 2006;65(5):1560-71.

45. Bergh L. Breathing adapted radiotherapy of breast cancer: Investigation of two different gating techniques and visual guidance, using optical surface scanning and pressure monitoring. Master of Science Thesis, Lund University. 2014. https://lup.lub.lu.se/student-papers/search/publication/4623050.
46. Cervino LI, Gupta S, Rose MA, Yashar C, Jiang SB. Using surface imaging and visual coaching to improve the reproducibility and stability of deep-inspiration breath hold for left-breast-cancer radiotherapy. Phys Med Biol. 2009;54(22):6853-65.
47. Schonecker S, Walter F, Freislederer P, Marisch C, Scheithauer H, Harbeck N, et al. Treatment planning and evaluation of gated radiotherapy in left-sided breast cancer patients using the CatalystTM/SentinelTM system for deep inspiration breath-hold (DIBH). Radiat Oncol. 2016;11(1):143.
48. Walter F, Freislederer P, Belka C, Heinz C, Sohn M, Roeder F. Evaluation of daily patient positioning for radiotherapy with a commercial 3D surface-imaging system (Catalyst). Radiat Oncol. 2016;11(1):154.
49. Stieler F, Wenz F, Shi M, Lohr F. A novel surface imaging system for patient positioning and surveillance during radiotherapy. A phantom study and clinical evaluation. Strahlenther Onkol. 2013;189(11):938-44.
50. Nutti B, Kronander Å, Nilsing M, Maad K, Svensson C, Li H. Depth sensor-based realtime tumor tracking for accurate radiation therapy. Eurographics. 2014:10-3.
51. Li H, Sumner R, Pauly M. Global Correspondence Optimization for Non-Rigid Registration of Depth Scans. Comput Graph Forum. 2008;27(5):1421-30.
52. Heinz C, Reiner M, Belka C, Walter F, Sohn M. Technical evaluation of different respiratory monitoring systems used for 4D CT acquisition under free breathing. J Appl Clin Med Phys. 2015;16(2):334-49.
53. Klein S, Staring M. Elastix the manual v4.8. 2015. http://elastix.isi.uu.nl/download/elastix_manual_v4.8.pdf.
54. Brock KK, Mutic S, McNutt TR, Li H, Kessler ML. Use of Image Registration and Fusion Algorithms and Techniques in Radiotherapy: Report of the AAPM Radiation Therapy Comittee Task Group No. 132. Med Phys. 2017;44(7):43-76.
55. Rietzel E, Chen GT, Choi NC, Willet CG. Four-dimensional image-based treatment planning: Target volume segmentation and dose calculation in the presence of respiratory motion. Int J Radiat Oncol Biol Phys. 2005;61(5):1535-50.
56. Keall P. 4-dimensional computed tomography imaging and treatment planning. Semin Radiat Oncol. 2004;14(1):81-90.
57. Feuvret L, Noel G, Mazeron JJ, Bey P. Conformity index: a review. Int J Radiat Oncol Biol Phys. 2006;64(2):333-42.
58. Paddick I. A simple scoring ratio to index the conformity of radiosurgical treatment plans. Technical note. J Neurosurg. 2000;93 Suppl 3:219-22.
59. Chaikh A, Giraud JY, Perrin E, Bresciani JP, Balosso J. The choice of statistical methods for comparisons of dosimetric data in radiotherapy. Radiat Oncol. 2014;9:205.
60. Baumann M, Petersen C. TCP and NTCP: a basic introduction. Rays. 2005;30(2):99-104.

61. Burman C, Kutcher G, Emami B, Goitein M. Fitting of normal tissue tolerance data to an analytic function. Int J Radiat Oncol Biol Phys. 1991;21:123-35.
62. Kallman P, Agren A, Brahme A. Tumour and normal tissue responses to fractionated non-uniform dose delivery. Int J Radiat Biol. 1992;62:249-62.
63. Kugele M, Edvardsson A, Berg L, Alkner S, Andersson Ljus C, Ceberg S. Dosimetric effects of intrafractional isocenter variation during deep inspiration breath-hold for breast cancer patients using surface-guided radiotherapy. J Appl Clin Med Phys. 2018;19(1):25-38.
64. Early Breast Cancer Trialists´ Collaborative Group. Effect of radiotherapy after breast-conserving surgery on 10-year recurrence and 15-year breast cancer death: meta-analysis of individual patient data for 10 801 women in 17 randomised trials. Lancet. 2011;378:1707-16.
65. Early Breast Cancer Trialists´ Collaborative Group. Effect of radiotherapy after mastectomy and axillary surgery on 10-year recurrence and 20-year breast cancer mortality: meta-analysis of individual patient data for 8135 women in 22 randomised trials. Lancet. 2014;383:2127-35.
66. Darby SC, McGale P, Taylor CW, Peto R. Long-term mortality from heart disease and lung cancer after radiotherapy for early breast cancer: prospective cohort study of about 300 000 women in US SEER cancer registries. Lancet Oncol. 2005;6(8):557-65.
67. Harris EE, Correa C, Hwang WT, Liao J, Litt HI, Ferrari VA, et al. Late cardiac mortality and morbidity in early-stage breast cancer patients after breast-conservation treatment. J Clin Oncol. 2006;24(25):4100-6.
68. Early Breast Cancer Trialists´ Collaborative Group. Effects of radiotherapy and of differences in the extent of surgery for early breast cancer on local recurrence and 15-year survival: an overview of the randomised trials. Lancet. 2005;366:2087-106.
69. Darby SC, Ewertz M, McGale P, Bennet AM, Blom-Goldman U, Brønnum D, et al. Risk of Ischemic Heart Disease in Women after Radiotherapy for Breast Cancer. N Engl J Med. 2013;368(11):987-98.
70. Giordano SH, Kuo YF, Freeman JL, Buchholz TA, Hortobagyi GN, Goodwin JS. Risk of cardiac death after adjuvant radiotherapy for breast cancer. J Natl Cancer Inst. 2005;97(6):419-24.
71. Boero IJ, Paravati AJ, Triplett DP, Hwang L, Matsuno RK, Gillespie EF, et al. Modern Radiation Therapy and Cardiac Outcomes in Breast Cancer. Int J Radiat Oncol Biol Phys. 2016;94(4):700-8.
72. van den Bogaard VA, Ta BD, van der Schaaf A, Bouma AB, Middag AM, Bantema-Joppe EJ, et al. Validation and Modification of a Prediction Model for Acute Cardiac Events in Patients With Breast Cancer Treated With Radiotherapy Based on Three-Dimensional Dose Distributions to Cardiac Substructures. J Clin Oncol. 2017;35(11):1171-8.
73. Boekel NB, Schaapveld M, Gietema JA, Russell NS, Poortmans P, Theuws JC, et al. Cardiovascular Disease Risk in a Large, Population-Based Cohort of Breast Cancer Survivors. Int J Radiat Oncol Biol Phys. 2016;94(5):1061-72.

74. Nilsson G, Holmberg L, Garmo H, Duvernoy O, Sjogren I, Lagerqvist B, et al. Distribution of Coronary Artery Stenosis After Radiation for Breast Cancer. J Clin Oncol. 2011;30(4):380-6.
75. McGale P, Darby SC, Hall P, Adolfsson J, Bengtsson N-O, Bennet AM, et al. Incidence of heart disease in 35,000 women treated with radiotherapy for breast cancer in Denmark and Sweden. Radiother Oncol. 2011;100(2):167-75.
76. Paszat LF, Mackillop WJ, Groome P, Schulze K, Holowaty E. Mortality from myocardial infarcion following postlumpectomy radiotherapy for breast cancer: a population-based study in Ontario, Canada Int J Radiat Oncol Biol Phys. 1999;43:755-62.
77. Marks LB, Bentzen SM, Deasy JO, Kong FM, Bradley JD, Vogelius IS, et al. Radiation dose-volume effects in the lung. Int J Radiat Oncol Biol Phys. 2010;76(3 Suppl):S70-6.
78. Henson KE, McGale P, Taylor C, Darby SC. Radiation-related mortality from heart disease and lung cancer more than 20 years after radiotherapy for breast cancer. Br J Cancer. 2013;108(1):179-82.
79. Taylor C, McGale P, Brønnum D, Correa C, Cutter D, Duane FK, et al. Cardiac Structure Injury After Radiotherapy for Breast Cancer: Cross-Sectional Study With Individual Patient Data. J Clin Oncol. 2018;36(22):2288-96.
80. Shah C, Badiyan S, Berry S, Khan AJ, Goyal S, Schulte K, et al. Cardiac dose sparing and avoidance techniques in breast cancer radiotherapy. Radiother Oncol. 2014;112(1):9-16.
81. Bergom C, Currey A, Desai N, Tai A, Strauss JB. Deep Inspiration Breath Hold: Techniques and Advantages for Cardiac Sparing During Breast Cancer Irradiation. Front Oncol. 2018;8:87.
82. Latty D, Stuart KE, Wang W, Ahern V. Review of deep inspiration breath-hold techniques for the treatment of breast cancer. J Med Radiat Sci. 2015;62(1):74-81.
83. Smyth LM, Knight KA, Aarons YK, Wasiak J. The cardiac dose-sparing benefits of deep inspiration breath-hold in left breast irradiation: a systematic review. J Med Radiat Sci. 2015;62(1):66-73.
84. Edvardsson A, Nilsson MP, Amptoulach S, Ceberg S. Comparison of doses and NTCP to risk organs with enhanced inspiration gating and free breathing for left-sided breast cancer radiotherapy using the AAA algorithm. Radiat Oncol. 2015;10:84.
85. Fagundes M, Hug EB, Pankuch M, Fang C, McNeeley S, Mao L, et al. Proton Therapy for Local-regionally Advanced Breast Cancer Maximizes Cardiac Sparing. Int J Particle Ther. 2015;1(4):827-44.
86. Flejmer AM, Nyström PW, Dohlmar F, Josefsson D, Dasu A. Potential Benefit of Scanned Proton Beam versus Photons as Adjuvant Radiation Therapy in Breast Cancer. Int J Particle Ther. 2015;1(4):845-55.
87. Lomax AJ, Cella L, Weber D, Kurtz JM, Miralbell R. Potential role of intensity-modulated photons and protons in the treatment of the breast and regional nodes. Int J Radiat Oncol Biol Phys. 2003;55(3):785-92.

88. Ares C, Khan S, Macartain AM, Heuberger J, Goitein G, Gruber G, et al. Postoperative proton radiotherapy for localized and locoregional breast cancer: potential for clinically relevant improvements? Int J Radiat Oncol Biol Phys. 2010;76(3):685-97.
89. MacDonald SM, Jimenez R, Paetzold P, Adams J, Beatty J, DeLaney TF, et al. Proton radiotherapy for chest wall and regional lymphatic radiation; dose comparisons and treatment delivery. Radiat Oncol. 2013;8:71.
90. Tommasino F, Durante M, D'Avino V, Liuzzi R, Conson M, Farace P, et al. Model-based approach for quantitative estimates of skin, heart, and lung toxicity risk for left-side photon and proton irradiation after breast-conserving surgery. Acta Oncol. 2017;56(5):730-6.
91. Oden J, Toma-Dasu I, Eriksson K, Flejmer AM, Dasu A. The influence of breathing motion and a variable relative biological effectiveness in proton therapy of left-sided breast cancer. Acta Oncol. 2017;56(11):1428-36.
92. Orecchia R, Fossati P, Zurrida S, Krengli M. New frontiers in proton therapy: applications in breast cancer. Curr Opin Oncol. 2015;27(6):427-32.
93. Depauw N, Batin E, Daartz J, Rosenfeld A, Adams J, Kooy H, et al. A novel approach to postmastectomy radiation therapy using scanned proton beams. Int J Radiat Oncol Biol Phys. 2015;91(2):427-34.
94. Stick LB, Yu J, Maraldo MV, Aznar MC, Pedersen AN, Bentzen SM, et al. Joint Estimation of Cardiac Toxicity and Recurrence Risks After Comprehensive Nodal Photon Versus Proton Therapy for Breast Cancer. Int J Radiat Oncol Biol Phys. 2017;97(4):754-61.
95. Mast ME, Vredeveld EJ, Credoe HM, van Egmond J, Heijenbrok MW, Hug EB, et al. Whole breast proton irradiation for maximal reduction of heart dose in breast cancer patients. Breast Cancer Res Treat. 2014;148:33-9.
96. Lin LL, Vennarini S, Dimofte A, Ravanelli D, Shillington K, Batra S, et al. Proton beam versus photon beam dose to the heart and left anterior descending artery for left-sided breast cancer. Acta Oncol. 2015;54(7):1032-9.
97. Flejmer AM, Edvardsson A, Dohlmar F, Josefsson D, Nilsson M, Witt Nystrom P, et al. Respiratory gating for proton beam scanning versus photon 3D-CRT for breast cancer radiotherapy. Acta Oncol. 2016;55(5):577-83.
98. Knoos T, Wieslander E, Cozzi L, Brink C, Fogliata A, Albers D, et al. Comparison of dose calculation algorithms for treatment planning in external photon beam therapy for clinical situations. Phys Med Biol. 2006;51(22):5785-807.
99. Fogliata A, Vanetti E, Albers D, Brink C, Clivio A, Knoos T, et al. On the dosimetric behaviour of photon dose calculation algorithms in the presence of simple geometric heterogeneities: comparison with Monte Carlo calculations. Phys Med Biol. 2007;52(5):1363-85.
100. Chung E, Corbett JR, Moran JM, Griffith KA, Marsh RB, Feng M, et al. Is there a dose-response relationship for heart disease with low-dose radiation therapy? Int J Radiat Oncol Biol Phys. 2013;85(4):959-64.

101. Gagliardi G, Lax I, Ottolenghi A, Rutqvist L. Long-term cardiac mortality after radiotherapy of breast cancer-application of the relative seriality model. Brit J Radiol. 1996;69:839-46.
102. Gagliardi G, Bjöhle J, Lax I, Ottolenghi A, Eriksson F, Liedberg A, et al. Radiation pneumonitis after breast cancer irradiation: analysis of the complication probability using the relative seriality model. Int J Radiat Oncol Biol Phys. 2000;46:373-81.
103. Hedin E, Bäck A. Influence of different dose calculation algorithms on the estimate of NTCP for lung complications. J Appl Clin Med Phys. 2013;14:127-39.
104. Tang X, Zagar TM, Bair E, Jones EL, Fried D, Zhang L, et al. Clinical experience with 3-dimensional surface matching-based deep inspiration breath hold for left-sided breast cancer radiation therapy. Pract Radiat Oncol. 2014;4(3):e151-8.
105. Tang X, Cullip T, Dooley J, Zagar T, Jones E, Chang S, et al. Dosimetric effect due to the motion during deep inspiration breath hold for left-sided breast cancer radiotherapy. J Appl Clin Med Phys. 2015;16(4):91-9.
106. Gierga DP, Turcotte JC, Sharp GC, Sedlacek DE, Cotter CR, Taghian AG. A voluntary breath-hold treatment technique for the left breast with unfavorable cardiac anatomy using surface imaging. Int J Radiat Oncol Biol Phys. 2012;84(5):e663-8.
107. Tseng YD, Cutter DJ, Plastaras JP, Parikh RR, Cahlon O, Chuong MD, et al. Evidence-based Review on the Use of Proton Therapy in Lymphoma From the Particle Therapy Cooperative Group (PTCOG) Lymphoma Subcommittee. Int J Radiat Oncol Biol Phys. 2017;99(4):825-42.
108. Haffty BG, Whelan T, P.M. P. Radiation of the internal mammaty nodes: Is there a benefit? J Clin Oncol. 2016;34(4):297-9.
109. Verma V, Vicini F, Tendulkar RD, Khan AJ, Wobb J, Edwards-Bennett S, et al. Role of Internal Mammary Node Radiation as a Part of Modern Breast Cancer Radiation Therapy: A Systematic Review. Int J Radiat Oncol Biol Phys. 2016;95(2):617-31.
110. Dasu A, Flejmer AM, Edvardsson A, Witt Nyström P. Normal tissue sparing potential of scanned proton beams with and without respiratory gating for the treatment of internal mammary nodes in breast cancer radiotherapy. Phys Med. 2018;52:81-5.
111. Flejmer AM, Chehrazi B, Josefsson D, Toma-Dasu I, Dasu A. Impact of physiological breathing motion for breast cancer radiotherapy with proton beam scanning - An in silico study. Phys Med. 2017;39:88-94.
112. Specht L, Yahalom J, Illidge T, Berthelsen AK, Constine LS, Eich HT, et al. Modern radiation therapy for Hodgkin lymphoma: field and dose guidelines from the international lymphoma radiation oncology group (ILROG). Int J Radiat Oncol Biol Phys. 2014;89(4):854-62.
113. Maraldo MV, Specht L. A decade of comparative dose planning studies for early-stage Hodgkin lymphoma: what can we learn? Int J Radiat Oncol Biol Phys. 2014;90(5):1126-35.
114. Engert A, Plütschow A, Eich HT, Lohri A, Dörken B, Borchmann P, et al. Reduced Treatment Intensity in Patients with Early-Stage Hodgkin´s Lymphoma. N Engl J Med. 2010;363:640-52.

115. Eich HT, Diehl V, Gorgen H, Pabst T, Markova J, Debus J, et al. Intensified chemotherapy and dose-reduced involved-field radiotherapy in patients with early unfavorable Hodgkin's lymphoma: final analysis of the German Hodgkin Study Group HD11 trial. J Clin Oncol. 2010;28(27):4199-206.
116. Lohr F, Georg D, Cozzi L, Eich HT, Weber DC, Koeck J, et al. Novel radiotherapy techniques for involved-field and involved-node treatment of mediastinal Hodgkin lymphoma: when should they be considered and which questions remain open? Strahlenther Onkol. 2014;190(10):864-71.
117. Fiandra C, Filippi AR, Catuzzo P, Botticella A, Ciammella P, Franco P, et al. Different IMRT solutions vs. 3D-Conformal Radiotherapy in early stage Hodgkin´s lymphoma: dosimetric comparison and clinical considerations. Radiat Oncol. 2012;7:186.
118. Voong KR, McSpadden K, Pinnix CC, Shihadeh F, Reed V, Salehpour MR, et al. Dosimetric advantages of a "butterfly" technique for intensity-modulated radiation therapy for young female patients with mediastinal Hodgkin's lymphoma. Radiat Oncol. 2014;9:94.
119. Edvardsson A, Kugele M, Alkner S, Enmark M, Nilsson J, Kristensen I, et al. Comparative treatment planning study for mediastinal Hodgkin´s lymphoma: Impact on normal tissue dose using deep inspiration breath hold proton and photon therapy. Acta Oncol. 2018; DOI: 10.1080/0284186X.2018.1512153.
120. Willett CG, Linggood RM, Stracher MA, Goitein M, Doppke K, Kushner DC, et al. The effect of the respiratory cycle on mediastinal and lung dimensions in Hodgkin's disease. Implications for radiotherapy gated to respiration. Cancer 1987;60(6):1232-7.
121. Stromberg JS, Sharpe MB, Kim LH, Kini VR, Jaffray DA, Martinez AA, et al. Active breathing control (ABC) for Hodgkin´s disease: reduction in normal tissue irradiation with deep inspiration and implications for treatment. Int J Radiat Oncol Biol Phys. 2000;48:797-806.
122. Paumier A, Ghalibafian M, Gilmore J, Beaudre A, Blanchard P, el Nemr M, et al. Dosimetric benefits of intensity-modulated radiotherapy combined with the deep-inspiration breath-hold technique in patients with mediastinal Hodgkin's lymphoma. Int J Radiat Oncol Biol Phys. 2012;82(4):1522-7.
123. Petersen PM, Aznar MC, Berthelsen AK, Loft A, Schut DA, Maraldo M, et al. Prospective phase II trial of image-guided radiotherapy in Hodgkin lymphoma: benefit of deep inspiration breath-hold. Acta Oncol. 2015;54(1):60-6.
124. Charpentier AM, Conrad T, Sykes J, Ng A, Zhou R, Parent A, et al. Active breathing control for patients receiving mediastinal radiation therapy for lymphoma: Impact on normal tissue dose. Pract Radiat Oncol. 2014;4(3):174-80.
125. Aznar MC, Maraldo MV, Schut DA, Lundemann M, Brodin NP, Vogelius IR, et al. Minimizing late effects for patients with mediastinal Hodgkin lymphoma: deep inspiration breath-hold, IMRT, or both? Int J Radiat Oncol Biol Phys. 2015;92(1):169-74.
126. Enmark M, Lundkvist N, Fager M, Kugele M, Nyström H, Ceberg S. PTC17-0493: Clinical Commissioning of Gated Proton Pencil Beam Scanning. Int J Particle Ther. 2017;4(2):177.

127. Nicolini G, Vanetti E, Clivio A, Fogliata A, Cozzi L. Pre-clinical evaluation of respiratory-gated delivery of volumetric modulated arc therapy with RapidArc. Phys Med Biol. 2010;55(12):347-57.
128. Qian J, Xing L, Liu W, Luxton G. Dose verification for respiratory-gated volumetric modulated arc therapy. Phys Med Biol. 2011;56(15):4827-38.
129. Riley C, Yang Y, Li T, Zhang Y, Heron DE, Huq MS. Dosimetric evaluation of the interplay effect in respiratoty-gated RapidArc radiation therapy. Med Phys. 2014;41(1):011715.
130. Viel F, Lee R, Gete E, Duzenli C. Amplitude gating for a coached breathing approach in respiratory gated 10 MV flattening filter-free VMAT delivery. J Appl Clin Med Phys. 2015;16(4):79-90.
131. Rechner LA, Maraldo MV, Vogelius IR, Zhu XR, Dabaja BS, Brodin NP, et al. Life years lost attributable to late effects after radiotherapy for early stage Hodgkin lymphoma: The impact of proton therapy and/or deep inspiration breath hold. Radiother Oncol. 2017;125(1):41-7.
132. Baues C, Marnitz S, Engert A, Baus W, Jablonska K, Fogliata A, et al. Proton versus photon deep inspiration breath hold technique in patients with hodgkin lymphoma and mediastinal radiation: A planning comparison of deep inspiration breath hold intensity modulation radiotherapy and intensity modulated proton therapy. Radiat Oncol. 2018;13(1):122.
133. Zeng C, Plastaras JP, Tochner ZA, White BM, Hill-Kayser CE, Hahn SM, et al. Proton pencil beam scanning for mediastinal lymphoma: the impact of interplay between target motion and beam scanning. Phys Med Biol. 2015;60(7):3013-29.
134. Li Y, Niemela P, Liao L, Jiang S, Li H, Poenish F, et al. Selective robust optimization: A new intensity-modulated proton therapy optimization strategy. Med Phys. 2015;42(8):4840-7.
135. Liu W, Zhang X, Li Y, Mohan R. Robust optimization of intensity modulated proton therapy. Med Phys. 2012;39(2):1079-91.
136. Enmark M, Olofsson J, Ceberg S, Jonsson J. [P205] The impact on pencil beam scanning (PBS) proton therapy for mediastinal lymphoma from deep inspiration breath-hold (DIBH) variability. Phys Med. 2018;52:159.
137. Court L, Wagar M, Ionascu D, Berbeco R, Chin L. Management of the interplay effect when using dynamic MLC sequences to treat moving targets. Med Phys. 2008;35(5):1926-31.
138. Poulsen PR, Schmidt ML, Keall PJ, Worm ES, Fledelius W, Hoffmann L. A method of dose reconstruction for moving targets compatible with dynamic treatments. Med Phys. 2012;39(10):6237-46.
139. Ceberg S, Ceberg C, Falk M, af Rosenschöld PM, Bäck SÅJ. Evaluation of breathing interplay effects during VMAT by using 3D gel measurements. J Phys Conf Ser. 2013;444:012098.
140. Ong CL, Dahele M, Slotman BJ, Verbakel WF. Dosimetric impact of the interplay effect during stereotactic lung radiation therapy delivery using flattening filter-free beams and volumetric modulated arc therapy. Int J Radiat Oncol Biol Phys. 2013;86(4):743-8.

141. Ong CL, Verbakel WF, Cuijpers JP, Slotman BJ, Senan S. Dosimetric impact of interplay effect on RapidArc lung stereotactic treatment delivery. Int J Radiat Oncol Biol Phys. 2011;79(1):305-11.
142. Li X, Yang Y, Li T, Fallon K, Heron DE, Huq MS. Dosimetric effect of respiratory motion on volumetric-modulated arc therapy-based lung SBRT treatment delivered by TrueBeam machine with flattening filter-free beam. J Appl Clin Med Phys. 2013;14(6):195-204.
143. Stambaugh C, Nelms BE, Dilling T, Stevens C, Latifi K, Zhang G, et al. Experimentally studied dynamic dose interplay does not meaningfully affect target dose in VMAT SBRT lung treatments. Med Phys. 2013;40(9):091710.
144. Ehrbar S, Lang S, Stieb S, Riesterer O, Stark LS, Guckenberger M, et al. Three-dimensional versus four-dimensional dose calculation for volumetric modulated arc therapy of hypofractionated treatments. Z Med Phys. 2016;26(1):45-53.
145. Hubley E, Pierce G. The influence of plan modulation on the interplay effect in VMAT liver SBRT treatments. Phys Med. 2017;40:115-21.
146. Kuo HC, Mah D, Chuang KS, Wu A, Hong L, Yaparpalvi R, et al. A method incorporating 4DCT data for evaluating the dosimetric effects of respiratory motion in single-arc IMAT. Phys Med Biol. 2010;55(12):3479-97.
147. Edvardsson A, Nordström F, Ceberg C, Ceberg S. Motion induced interplay effects for VMAT radiotherapy. Phys Med Biol. 2018;63(8):085012.
148. Nordström F. Quality Assurance in Radiotherapy - Development and evaluation of new tools for improved patient safety. Doctoral thesis, Lund University, ISBN 978-91-7473-271-9, 2012.
149. Nordström F, af Wetterstedt S, Bäck SÅJ. 4D dosimetry and its applications to pre-treatment quality control and real-time in vivo dosimetry of VMAT treatments. J Phys Conf Ser. 2013;444:012021.
150. Lujan AE, Larsen EW, Balter JM, Ten Haken RK. A method for incorporating organ motion due to breathing into 3D dose calculations. Med Phys. 1999;26:715-20.
151. Poulsen PR, Worm ES, Petersen JB, Grau C, Fledelius W, Hoyer M. Kilovoltage intrafraction motion monitoring and target dose reconstruction for stereotactic volumetric modulated arc therapy of tumors in the liver. Radiother Oncol. 2014;111(3):424-30.
152. Worm ES, Hoyer M, Fledelius W, Hansen AT, Poulsen PR. Variations in magnitude and directionality of respiratory target motion throughout full treatment courses of stereotactic body radiotherapy for tumors in the liver. Acta Oncol. 2013;52(7):1437-44.
153. Kirilova A, Lockwood G, Choi P, Bana N, Haider MA, Brock KK, et al. Three-dimensional motion of liver tumors using cine-magnetic resonance imaging. Int J Radiat Oncol Biol Phys. 2008;71(4):1189-95.
154. Ge J, Santanam L, Noel C, Parikh PJ. Planning 4-dimensional computed tomography (4DCT) cannot adequately represent daily intrafractional motion of abdominal tumors. Int J Radiat Oncol Biol Phys. 2013;85(4):999-1005.

Dosimetric effects of breathing motion in radiotherapy

During radiotherapy, patients are treated using ionizing radiation with the aim to eradicate the tumour while sparing surrounding healthy tissue. This may be compromised for treatment in the thorax and abdomen because of breathing motion, resulting in a degradation of the dose distribution to the tumour and healthy tissue. Treatment during controlled deep inspiration could mitigate the motion and lead to favourable anatomical changes in the tumour position with respect to healthy tissue. In the work presented in this thesis, various effects of breathing motion on the tumour and healthy tissue dose distribution in photon and proton therapy were investigated.

Printed by Media-Tryck, Lund 2018 NORDIC SWAN ECOLABEL 3041 0903

LUND UNIVERSITY

FACULTY OF SCIENCE

Lund University
Faculty of Science
Department of Medical Radiation Physics
ISBN 978-91-7753-804-2

9 789177 538042